EFFECT OF BASALT MICROFIBERS ON THE SHEAR RESPONSE OF BFRP RC SHORT BEAMS

by

Mohamad Kusay Ahmad Rabee Sabbagh

A Thesis Presented to the Faculty of the:
American University of Sharjah
College of Engineering
in Partial Fulfillment
of the Requirements
for the Degree of:

Masters of Science in
Civil Engineering

Sharjah, United Arab Emirates

December 2019

Approval Signatures

We, the undersigned, approve the Master's Thesis of Mohamad Kusay Ahmad Rabee Sabbagh.

Thesis Title: Effect of Basalt Microfiber on the Shear Response of RC Short Beams.

Signature	**Date of Signature** (dd/mm/yyyy)
_____	_____
Dr. Farid Abed Professor, Department of Civil Engineering Thesis Advisor	
_____	_____
Dr. Adil Al-Tamimi Professor, Department of Civil Engineering Thesis Committee Member	
_____	_____
Dr. Wael Abuzaid Assistant Professor, Department of Mechanical Engineering Thesis Committee Member	
_____	_____
Dr. Irtishad Ahmad Head, Department of Civil Engineering	
_____	_____
Dr. Lotfi Romdhane Associate Dean for Graduate Affairs and Research College of Engineering	
_____	_____
Dr. Naif Darwish Acting Dean, College of Engineering	
_____	_____
Dr. Mohamed El-Tarhuni Vice Provost for Graduate Studies	

Acknowledgment

Foremost, I would be glad to express my heartfelt gratitude to my advisor Dr. Farid Abed for his continues guidance and supervision through my master study and thesis research. I am indebted to his immense knowledge and valuable assistance that were the main reasons helped me in accomplishing of this research.

My endless appreciation also goes to my thesis committee members Dr.Adil Al-Tamimi and Dr.Wael Abuzaid for their precious comments, advises and feedback assessment. In addition, I would like to thank Eng. Arshi Faridi and Eng. Mohamad Ansari who helped me in preparing research equipment and performing the lab work.

Also, I would like to acknowledge the financial support provided by the AUS (grant #: IRF002).

Dedication

I dedicate this accomplishment to my beloved parents, sister, brother and my future wife for the love, encouragement, sacrifices they gave me and for their endless support.

Abstract

Basalt composites are known for their high strength, lightweight and corrosion-resistance features. Basalt microfibers in fiber reinforced concrete mixes (FRC) can enhance the tensile strength, toughness and ductility as well as the post-cracking behavior of concrete members. This research investigates experimentally and analytically the effects of using basalt microfibers on the shear response of (FRC) short beams reinforced with basalt fiber reinforced polymers bars (BFRP), and compares the results with the strut-and-tie modeling (STM) according to ACI-318-14. The experimental program consists of performing four-point bending tests on eight BFRP-FRC short beams that are 2000 mm long with 150 mm x 260 mm cross-section each. The test parameters include shear span-to-depth ratio, reinforcement ratio, concrete compressive strength and the type of microfibers used in the concrete mix. Experimental results showed that the presence of basalt microfibers has a significant influence in enhancing the overall beam stiffness and ultimate shear strength of tested beams. The maximum load carrying capacity increased by 42.1% and 38.2% with addition of basalt and synthetic microfibers, respectively. The capability of basalt microfibers in improving the shear responses of tested beams is attributed to their ability in bridging the micro-cracks by the efficient transfer of the stresses from tips of those cracks to the surrounding concrete. Hence, the propagation of more cracks is eliminated and the failure in the beam is delayed, which results in a greater load-carrying capacity. The constructed STM model as per ACI 318-14 resulted in a conservative prediction of the ultimate shear strength of tested beams compared to the experimental results.

Keywords: ***Short beams; BFRP bars, Basalt fibers, Synthetic fibers, Fiber reinforced concrete; Shear strength, crack behavior.***

Table of Contents

List of Figures

List of Tables

List of Abbreviations

ACI	American concrete institution
AFRP	Aramid fiber reinforced polymer
ASTM	American Society of Testing and Materials
BFRC	Basalt fiber reinforced concrete
BFRP	Basalt fiber reinforced polymer
CFRP	Carbon fiber reinforced polymer
CSA	Canadian standards association
FBD	Free body diagram
FRP	Fiber reinforced polymer
GFRP	Glass fiber reinforced polymer
HBFRC	High strength basalt fiber reinforced concrete
JSCE	Japanese society of civil engineers
LVDT	Linear variable deferential transformer
NRC	Normal reinforced concrete
RC	Reinforced concrete
SFRC	Synthetic fiber reinforced concrete
STM	Strut and tie method
UTM	Universal testing machine

Chapter 1. Introduction

This chapter starts with a brief explanation of the shear behavior in short beams in general, followed by a brief outline of different reinforcement types in comparing with basalt fiber-reinforced polymers (BFRP) rebars. The chapter then presents the advantages of using FRP bars along with some examples of real-life applications. This is followed by a discussion of the effect of integrating the microfibers into concrete mixes. Finally, the problem statement, research significance and the objectives and structure of the research are explained.

1.1. Overview

Using new FRP composite materials to enhance the shear capacity of concrete beams is a new direction in the research industry. In order to improve the shear capacity of concrete, the shear behavior of each type of concrete beam should be understood. In general, the shear behavior of concrete beams is known to be influenced by the shear span-to-depth ratio (a/d) [1]. According to the American concrete institution ACI 318-14, a beam is categorized as a short beam if its clear span does not exceed four times of the overall beam depth (h) or if its shear span to effective depth ratio is equal or less than 2.5; otherwise, it is considered a slender beam [2]. The behavior of slender concrete beams is known to be governed by the beam action while the contribution of the arch actions to the shear strength of those beams is insignificant [1]. Based on the shear span to depth ratio, the overall strength of short or deep beams is generally controlled by shear rather than flexure if a normal amount of reinforcement is used and the shear strength and behavior of short concrete beams is mainly influenced by arch action [3].

Concrete and steel are used together as main building materials for their high compressive strength, good durability and low cost [4][5]. It is well known that concrete is a quasi-brittle material and has a limited tensile strength. Therefore, using reinforcing steel bars on the tension side of concrete structures is the conventional technique to increase their tensile strength. However, conventional steel rebars have many weaknesses in the construction industry such as their susceptibility to corrosion when exposed to aggressive moisture and chemicals [4]. When steel bars corrode, their tensile strength decreases and the stress on steel-reinforced concrete parts increases, initiating

cracks and causing spall in the concrete that leads to faster deterioration. If this process is allowed to continue, it could compromise the entire structure's integrity. Structures facing corrosion necessitate costly maintenance and repair work [4]. In a study of corrosion problem done by Koch et al., it was shown that the annual direct cost of corrosion on US highway bridges is estimated as $8.3 billion, with an overall $4.0 billion in capital costs for maintenance and repair works of concrete bridge decks and substructures [6]. It is well known problem in the countries that characterized by warm climate and humidity conditions, especially in the marine areas. in addition to harm weather conditions and humidity, the saline ground waters, increases all corrosion problems [4].

In the past few decades, the demand on advanced construction materials that help in solving corrosion and deterioration problems has increased. (FRP) are one of those advanced materials that are increasingly being considered as an enhanced reinforcement to substitute conventional steel in structural elements [7]. The process of corrosion and its products damage the interface between reinforcing bars and concrete, thus reducing the bond strength, and eventually, shortening the service life of concrete structures [8]. The corrosion-resistance feature in FRP bars marks it as a main solution for corrosion and chemical threats faced by structural steel elements[9][10][11]. In general, FRP composites consist of two main components: fibers and a polymer matrix. The fibers comprise 30-70% of the volume of the components [12]. The main role of fibers in the composite is to carry the load and provide strength, stiffness and other mechanical properties [12]. The matrix works to ensure the position and alignment of the internal fibers as well as to protect from damages during manufacturing. It is also responsible for composite durability and protection from harm environmental conditions[12].

In addition to their corrosion resistance, FRP composites are characterized by their non-conductivity, light weight, high specific strength and stiffness [12]. Due to these advantages, FRP composites have been introduced as a new reinforcement alternative that can be tailored to satisfy concrete design criteria [13]. FRP bars have the potential to be used as main reinforcement in many concrete structures such as bridge decks, floor slabs, abutments and footings[14]. The last application is the most beneficial as FRP bars have good resistance to corrosion and chemical attacks[15].

Figure 1 and 2 show the use of glass fiber reinforced polymer bars as a main bridge deck and Metrorail reinforcement in Manitoba city and Miami state [16].

Figure 1: The 18th street bridge deck reinforced with GFRP bars in Manitoba [10]

Figure 2: Miami-dade metrorail project used GFRP bar reinforcement [10]

There are three main types of FRP composites: Carbon fiber reinforced polymer (CFRP), Glass fiber reinforced polymer (GFRP) and Aramid fiber reinforced polymer (AFRP) [17][18]. Recently, Basalt fiber has been introduced to the construction industry in the form of a new promising reinforcement material known as Basalt Fiber Reinforced Polymer (BFRP) [17]. Recent comprehensive studies, such as those conducted by Ovitigala and Issa, Tomlinson and Fam El Refai and Abed.[19][20][17], have been conducted to study the behavior of basalt fiber as a reinforcement material. Such studies will be discussed in the literature review section. In short, basalt fiber

reinforced polymer BFRP bars are expected to have characteristics that are more beneficial with significant cost reduction compared to other FRP composites. For instance, BFRP bars have a higher strength and modulus of elasticity as well as more chemical stability than GFRP [21]. Additionally, they have a higher temperature resistance and lower cost than CFRP. Practically, FRP composites have a lower modulus of elasticity than that of conventional steel bars, which considered as main disadvantage of using FRP composites, and tends to increase the deformation in beams and hence leads to a wider crack width. For example, GFRP and AFRP have a modulus of elasticity of 35-50 GPa, while the conventional steels have one of 200 GPa [2]. Furthermore, the tensile behavior in FRP is higher than that in conventional steel. FRP composites exhibit a linear stress-strain relationship until rapture; therefore a ductile failure similar to that of beams reinforced with conventional steel does not occur in concrete beams reinforced with FRP bars [2].

Due to the differences in properties between FRP bars and conventional steel bars such as modulus of elasticity, tensile strength and bond characteristics, the shear behavior of concrete beams reinforced with FRP reinforcement is expected to be different than that of concrete beams reinforced with steel bars. Many studies have been conducted on both slender and short beams, reinforced with different types of FRP bars, to study the shear behavior of these beams. Razaqpur et al. [22] investigated the shear behavior of slender beams reinforced with FRP bars and reported a reduction in shear strength for such members in comparison with other beams that have the same steel reinforcement ratios of conventional steel. This reduction in shear strength in slender beams was attributed mainly to the low modulus of elasticity in FRP bars [23]. On the other hand, since short beams have different shear mechanisms than slender beams, as illustrated before, the influence of using BFRP bars as a main reinforcement material in short beams is yet to be fully understood.

Another approach that has recently been used to enhance the shear capacity of concrete beams is the use of Macro and Micro fibers as an advanced content in concrete mixes. Fibers have a potential to enhance the post-cracking behavior of concrete beams. Specifically, shear strength, toughness and ductility of concrete beams is enhanced by the improved material properties of FRC members. Their main purpose is to increase the tensile and flexural strengths of concrete structures [24]. The effect of fibers on the

shear behavior of concrete beams can be summarized in two main factors. First, it has a direct influence imposed by the post-cracking strength when inclined shear crack is taking place. Second, it has an indirect role in improving the contribution of concrete to shear strength through the dowel action in longitudinal reinforcement [24]. Many researches have studied the behavior of FRC as will be illustrated in the literature review section. The results of all studies on different types of fibers used in FRC showed that fibers help boost the shear capacity as well as improve the shear crack resistance.

1.2. Problem Statement

To date, a limited number of studies have been conducted to investigate the effect of Basalt microfibers on the shear behavior of concrete beams reinforced with Basalt fiber reinforced polymers (BFRP) bars. In contrast, many studies have been performed to understand the characteristics of plain concrete beams reinforced with other types of FRP such as GFRP and CFRP rebars and to investigate the effect of adding steel, glass and synthetic microfibers on short concrete beams. The reason for that is, mainly, the lack of knowledge about the structural behavior of the new Basalt microfibers and BFRP bars, especially since most concrete structure design guidelines and American standards do not include specific provisions for BFRP like other FRP composites [17]. As illustrated earlier, BFRP bars have a corrosion resistance advantage and higher tensile strength than the steel bars. However, FRP bars do not yield as steel bars due to the micro-bulking of internal fibers and beams reinforced with FRP bars have a brittle behavior [25][26]. This causes a larger deformation in comparison to steel bars, resulting in larger crack-width. Wide cracks are considered the biggest risk in concrete structures due to their harmful role in allowing the penetration of water and chemicals, which attack the reinforcement directly, into the concrete. This point is largely considered as the negative side of using the FRP bars instead of steel rebars.

It is hence important to find an appropriate solution to overcome that drawback and make BFRP a possible replacement for conventional steel bars. In this research, the expected outcome of using microfibers is that these fibers will bridge the wide cracks and, consequently improve the shear capacity of short beams that reinforced with BFRP bars. This will decrease the crack width and lead to the enhancement of the strength and durability of BFRP reinforced concrete. These goals can be achieved by using

different types of microfibers such as basalt and synthetic microfibers. This research aims to understand the benefits behind using Basalt microfibers in reinforced concrete beams, outline their advantages, illustrate their effects on improving shear response in general and post-cracking behavior in particular, and compare them to other fiber types such as synthetic fibers.

1.3. Research Significance

The advances in materials technologies have raised the need of intensive researches on developing cost-effective and friendly materials to overcome the different problems and deterioration of concrete elements in the construction industry. The researches on fiber reinforced concrete that reinforced with different types of FRP bars have been increased because of their proven and effective advantages such as their corrosion resistance and non-conductivity. Lately, basalt fiber reinforced polymer bars (BFRP) have shown promising mechanical characteristics that are more comparable and beneficial than other FRP reinforcement types, while being meaningfully more cost-effective.

Reinforced concrete deep beams are known by their enormous structural applications such as buildings and bridges foundation, transfer girders and marine structures. The experimental evaluation of shear behavior of deep beams reinforced with FRP bars and casted along with fiber reinforced concrete (FRC) is found to be limited. This increases the need of more research related to deep BFRC beams reinforced with BFRP bars, since that the shear performance of BFRP bars has substantial acceptance in many structural elements in comparing with other FRP reinforcement materials.

In this research, the results of using different types of microfibers, shear span-to-depth ratios, reinforcement rations and concrete compressive strengths on the shear response of concrete short beams reinforced longitudinally with BFRP bars are explored. The study comprises both experimental and analytical work by using strut and tie model and assessing its applicability to evaluate the effect of microfibers on the shear response of BFRP-FRC short beams in accordance to ACI-318-14. According to the small shear span to depth ratio and arch action, the ultimate shear strength of deep beams is generally controlled by shear rather than flexural. The significance of this

study is roll mainly about evaluating the shear response of BFRP bars and basalt microfibers combination in BFRP-FRC short beams. That combination makes it a homogenous structure and an interesting system to be investigated, in order to overcome the low ductility of FRP bars and the severe deterioration problems of conventional steel reinforced concrete.

1.4. Research Objectives

The main objective of this thesis is to study the effect of Basalt microfibers on the shear response of short beams reinforced with BFRP bars. The main parameters of this study are the different types of microfibers (basalt and synthetic), different longitudinal reinforcement ratios of BFRP bars (ρ), the different shear span-to-depth ratios of concrete beams (a/d) and the different concrete compressive strengths (f'c). Experimental tests and numerical calculations will be conducted to investigate the following:

1- The effect of integrating basalt microfibers in concrete mix (FRC) on the shear behavior of BFRP-FRC short beams in comparison to other types of microfibers such as synthetic microfibers.
2- The effect of shear span-to-depth ratio on the shear behavior of BFRC-FRC short beams.
3- The effect of reinforcement ratios of BFRP bars on the shear behavior of short BFRP-FRC beams.
4- The effect of concrete compressive strength on the shear behavior of BFRP-FRC short beams.
5- The capability of the strut-and-tie model of ACI-318-14 in predicting the shear capacity of short FRC beams reinforced with BFRP bars.

1.5. Thesis Structure

The thesis starts with introduction chapter that introduces BFRP bars and basalt microfibers and mentioning their potential advantages when being used in one system. The chapter also points out the problem that being investigated and clarifies the significance of the study. The second chapter contains necessary background information to understand different important properties of the materials used in this study, such as BFRP bars, FRC and basalt microfibers. Moreover, Chapter 2 also shows

and discusses different research outcomes that conducted by others on studying the shear response of short beams reinforced longitudinally without web reinforcement with materials similar to BFRP, such as GFRP and CFRP. In addition, it discussed some of research findings on slender beams reinforced with BFRP bars and short FRC beams. Chapter 3 defines the experimental program in details. It presents the test matrix, test setup and instrumentation for the four-point bending test. The material evaluation and experimental programs results are summarized and presented in chapter 4, and then discussed in chapter 5 in order to understand the main contribution of the basalt microfibers in enhancing the shear behavior of BFRP short beams. Chapter 5 also evaluates the current strut and tie method according to ACI-318-14 in predicting the shear strength of BFRP-FRC short beams. The thesis ends in chapter 6, which includes the most significant conclusions that have been drawn from both experimental and analytical wok on the tested beams.

Chapter 2. Background and Literature Review

In this chapter, the mechanical and physical properties of different types of FRP bars are discussed, with focus on BFRP bars. Then, the shear behavior of short beams is explained and the related studies on the shear behavior of short beams reinforced with GFRP and CFPR as well as those on the shear behavior of slender concrete beams reinforced with BFRP bars are reviewed from literature. Finally, the contribution of microfibers on enhancing the shear performance of concrete beams is explained.

2.1. Fiber Reinforced Polymer (FRP) Properties

FRP composite material is defined as a polymer matrix that is reinforced with a different type of fiber. A multiphase material is produced by combining polymer matrix resins such as vinyl-ester, polyester and epoxy with reinforcing fibers, typically glass, aramid, carbon or basalt. Multiphase material is a new bulk material with more advanced properties than the individual base materials [27]. Structural elements that are made of FRP composites have been shown to provide efficient and economical characteristics due to their lightweight, noncorrosive, nonmagnetic and non-conductive properties. Furthermore, FRP composites show excellent energy absorption, a feature that can be suitable for seismic response and high fatigue strength conditions [28]. In addition to the high strength to weight ration of the FRP bars, concrete structures reinforced with those bars are less susceptible to harmful environmental conditions such as chemical attacks from soil, are considered to be more durable and require less repair and maintenance work than elements reinforced with conventional steel bars [29]. All of these characteristics of FRP bars make them an attractive reinforcement solution to all concrete structural elements in general and those subjected to severe environmental exposures in particular.

In general, FRP composites are considered as anisotropic materials since their properties vary as a function of direction. Their mechanical properties depend on the composite design specifications such as fiber orientation, diameter, volume, thickness and number of laminations. This engineering flexibility in FRP composites allows the designer to optimize design parameters based directly on the structural element requirements [30]. The upcoming sections discuss the major distinctive properties of FRP bars with focus on BFRP properties in comparison to other types of FRP bars. The

pictures shown in Figure 3 show examples of different types of reinforcement (steel and FRP bars) [31]-[32].

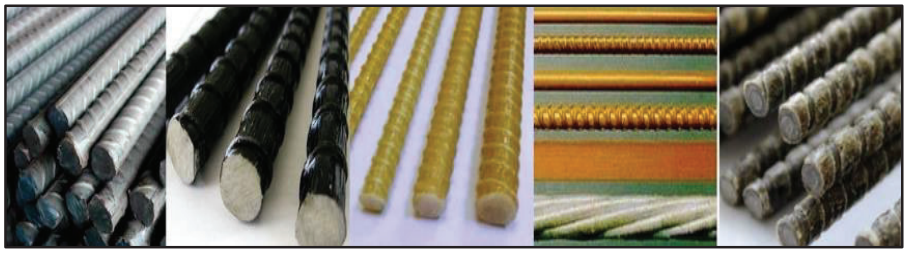

(a) (b) (c) (d) (e)

Figure 3: FRP composites: (a) ribbed steel, (b) ribbed CFRP bars, (c) ribbed GFRP bars, (d) ribbed AFRP bars and (e) ribbed BFRP bars [19, 20]

2.1.1. Shear strength of FRP composites. Shear stress in FRP composites can be described as in-plane shear stress happening through the thickness of the individual laminas. The internal shear resistance in concrete may be defined as a resistance in the fiber structure, which will vary depending on the type and volume of the fibers and the chosen test method [30]. Most FRP composite bars are relatively weak in shear between the internal laminar due to absence of reinforcement across the layers. The orientation of fibers across the fiber layers can enhance the shear resistance [2]. In comparison with GFRP and CFRP, BFRP have a greater strength than CFRP of equivalent production cost [33] and a higher chemical stability than GFRP of equivalent cost [33]. Furthermore, BFRP bars are observed to be five times stronger than low-carbon conventional steel [33].

2.1.2. Compressive strength of FRP composites. FRP composites that are subjected to a compression load may end up with different failures modes such as elastic micro bulking, shear splitting and global elastic bulking. There is no evidence in technical literature proving time-dependent creep for an FRP composite coupon subjected to compression [2]. Usually, the governing failure mode for a given FRP composite under compressive loading is predicted experimentally for a given fiber and matrix combination with distinct geometry [30]. In general, the compressive strength of FRP bars is usually lower than their tensile strength [34]. In recent studies, it was found that the compressive strength of AFRP, CFRP and GFRP bars are about 10%, 30-50% and 30-40% of their tensile strengths, respectively [35].

2.1.3. Tensile strength and modulus of elasticity of FRP composites. FRP composite materials are used as good tensile reinforcement in concrete beams. Research has proven that FRP bars have linear stress-strain behavior until failure [12]. Moreover, FRP bars have, in general, a lower modulus of elasticity than that of conventional steel by around 20% to 30% [3]. This is mainly attributed to the early-unpredicted rupture failure that results from end boorming and internal micro-bulking in the fibers under compression loads [2]. The tensile strength in FRP composites depends mainly on the type of fiber and matrix used in the composite but, in general, the tensile strength is much higher in FRP composites than in conventional steel [36]. In Figure 4, it was noticed that Basalt fiber reinforced polymers BFRP are generally between Glass fiber reinforced polymers GFRP and Carbon fiber reinforced polymers CFRP and more close to the Aramid fiber reinforced polymers in both stiffness and strength [20].

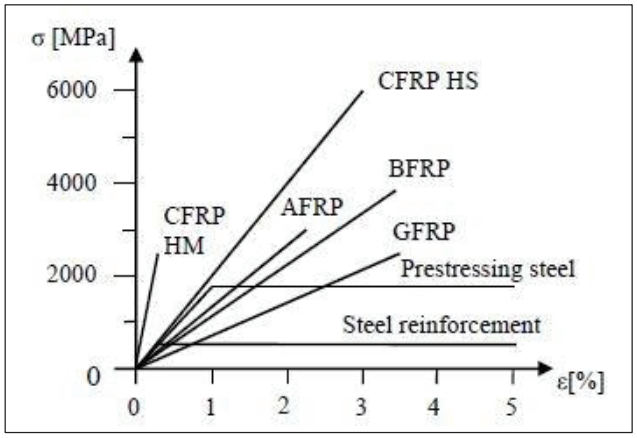

Figure 4: Stress-Strain diagram for steel and different FRP bars. [9]

2.1.4. Bond strength of FRP composites with concrete. The main aspect toward the worldwide acceptance of BFRP bars is their bond durability between concrete and FRP bars, since that the good bond dictates the overall ductility integrity of concrete member [37]. The bond strength of FRP bars to concrete can be attributed to the adhesion resistance of the bars' interface, which is defined as the chemical and fractional resistance of that interface against slipping, and to the mechanical interlock between the rebar and concrete interfaces [38].

Yan et al. have conducted a comprehensive study investigating the bond strength of GFRP bars. A database of 682 specimens was created. The specimens tested under the pullout test to understand the factors affecting the bond strength. The results showed a linear relationship between bond strength and concrete strength, assuming a constant concrete cover and a constant bar size [8].

Another study conducted by Elrefai et al. [39] aimed to examine the bond behavior of BFRP. 36 concrete cylinders were reinforced with either BFRP and another 12 concrete cylinders were reinforced with GFRP for comparison. Both sets were tested using the direct pullout test. The results revealed that concrete cylinders reinforced with BFRP bars develop a bond strength equivalent to 75% that of GFRP bars. The failure of BFRP cylinders was along the interfacial surface of the outer layer of the bars and along the core layer of the concrete [39].

2.2. Short Beams

The use of reinforced concrete short beams has become more common in recent years. The beams can be used in a variety of applications such as transfer beams in high-rise buildings, pile caps, foundation retaining walls, shear walls and floor diaphragms [40]. There are multiple definitions for reinforced concrete short beams given by different standards and researchers. Patil et al. were defined short beams as structural elements with large depth to span ratios [41].

The Canadian Standard Association CSA A23.3-04 defines beams that have clear-span to depth ratios of less than 2 as deep flexural members and states that these beams' non-linear distribution of strains should be taken into consideration in designing the structural elements [42]. The ACI 318-14 defines short beams as members with effective length less than four times the overall depth or beam regions on which a concentrated load is applied at a distance from the support less than or equal to twice the beam's depth, which needed to develop a compression area struts between loads and supports[43].

The shear behavior of short beams is different than that of normally reinforced beams and hence entails different design requirements, a more extensive analysis and greater reinforcement detailing. Short or deep beams are generally classified as non-

flexural elements. This is due to the fact that plane sections do not stay plane in bending. Hence, the principles of stress analysis for normal beams are not adequate to determine the shear strength of deep beams. Another important characteristic of deep beams is their high shear strength, which can be attributed to internal arch action. Arch action transfers the load directly to the supports through concrete struts. The reinforcement in short beams act as a tie in a simple short beam and in consequence, the concrete beam becomes similar to a steel truss.

The strain in short or deep beams is classified as non-linear. Stresses in short beams can be studied using methods of two-dimensional elasticity such as finite element methods. In short beams, the combination of concentrated loads and support reactions creates large compressive stresses at a right angle to the beams' axis. A complex stress field is hence formed in the webs of the beams as a result of the interaction between the loads and reactions. As the horizontal distance between the applied loads and support reactions (a/d ration) changes, the previously-mentioned stresses result in arch actions towards the supports. Because of the complexity of web stresses, understanding the shear behavior of short or deep beams is essential for safe and complete designs [44].

2.3. Literature Review

2.3.1. Shear behavior of concrete deep beams reinforced with GFRP & CFRP. Fibers such as carbon and glass are abundant, renewable, lightweight and have low density and high toughness. These fibers are used in forming CFRP and GFRP, respectively, which have the potential to be used as a direct replacement for conventional steel reinforcement, especially for applications that require a higher strength. A direct comparison between CFRP and GFRP has shown that the tensile and flexural strengths of CFRP composites are relatively higher than those of GFRP [45]. The following studies were conducted to examine the shear behavior of CFRP and GFRP composites as shear reinforcement bars in concrete deep beams.

In 2012, ElSayed et al. conducted a comparative study between CFRP and GFRP to evaluate the shear strength of fiber reinforced concrete deep beams [1]. The experimental program comprised of ten FRP-reinforced concrete beams of identical dimensions of 2600 mm length, 250 mm width and 400 mm depth tested under four-

point bending. The investigation test variables were reinforcement ratio ρ, modulus of elasticity of FRP bars and shear span-to-depth (a/d) ratio. The test results describe the behavior of deep beams in terms of load versus deflection response, modes of failure, crack patterns, strain in the reinforcement and concrete and ultimate shear capacity.

The test showed that, for a constant type of reinforcing material (CFRP or GFRP), the post-cracking stiffness increases as the reinforcement ratio ρ increases, and the rigidity increases as the span to depth ratio a/d decreases. Furthermore, flexural cracks were observed in early loading stages of the test, followed by inclined cracks at mid height between the loading point and supports before reaching the maximum load capacity. All beams reinforced with either CFRP or GFRP experienced a redistribution of internal stresses after inclined cracks were formed as a result of arch action. Most of the beams failed in diagonal splitting mode. After cracking, the beams reinforced with GFRP showed a larger strain compared to the beams reinforced with CFRP and this can be attributed to the lower modulus of elasticity of GFRP relative to that of CFRP. The development of arch action in the tested deep beams gives them the potential to develop an ultimate shear resistance over inclined cracks by more than 95-198% depending on the a/d ration.

In addition, the test showed that the ultimate shear strength increases significantly with the decrease of the a/d ration. For instance, decreasing a/d by 23% (from 1.69 to 1.30) increased shear strength of beams reinforced with CFRP and GFRP by 91% and 54%, respectively [1]. This increase can be attributed to the fact that tied arch action is more effective at lower a/d ratios since the angle between the inclined strut and longitudinal beam axis is higher.

Moreover, the ultimate shear strengths also increased with increases in the reinforcement ratio for both material reinforcement types. In general, deep beams reinforced with CFRP bars showed higher ultimate shear strengths than beams reinforced with GFRP bars, demonstrating the effect of the modulus of elasticity on the strength of fiber-reinforced polymer bars.

In another comparative study, Abed and AlHamaydeh [46], studied the shear of deep concrete beams reinforced with GFRP bars without any web reinforcement and compared it with similar steel reinforced beams. A total of 13 beams, of which nine

were reinforced with GFRP bars and four with conventional steel bars, with constant lengths of 2000 mm and widths and 200 mm, were tested with four-point bending test until failure.

The study aimed to explore the ultimate shear capacity as well as investigated the load deflection of the beams and the effect of shear span to depth ratio, reinforcement ratio, beam effective depth and concrete compressive strength on the ultimate shear behavior.

The experimental results showed that the overall stiffness of steel-reinforced concrete beams is higher than that of beams reinforced with GFRP bars. This is due to the low axial stiffness of fiber-reinforced polymer glass. In addition, the GFRP reinforced beams showed larger mid-span deflections compared to the steel reinforced beams due to the low modulus of elasticity of GFRP bars, which causes wider cracks. Increasing the reinforcement ratio ρ was found to improve the shear behavior and span length to depth ratio of all the beams.

Shear behavior improvement was also apparent in all beams with small a/d ratios, mainly because of the increase in the angel between the diagonal compression struts and the tension ties. The study concluded that the GFRP reinforced beams showed shear strength 50% higher than that of beams reinforced with conventional steel [46].

However, since the GFRP reinforced beams showed a comparably higher ultimate shear capacity than their steel reinforced counterparts, the test concluded that for deep beams the type of reinforcement material was not an influential factor for the occurrence of arch action mechanism and for ultimate shear strength capacity.

Farghaly and Benmokrane [47] studied the shear behavior of four full-scale deep beams reinforced in flexure with either CFRP or GFRP bars and with no shear reinforcement. The specimens all had 3000 mm span lengths with cross sections of 300 mm width and 1200 mm depth and were tested under four-point bending test. The primary test variables were the longitudinal reinforcement ratio ρ and the reinforcement type. The specimens hence had different moduli of elasticity and tensile strengths. The results were compared to those of the strut and tie method in accordance to ACI and CSA codes, demonstrating the importance of considering the effect of web reinforcement and the effect of axial stiffness on longitudinal reinforcement.

The experimental results illustrated that all the beams exhibited bilinear response until failure. The failure of all beams was brittle and characterized by diagonal shear failure mode followed directly by concrete crushing at the top of the diagonal struts. It was concluded that reinforcement ratio has no effects on the cracking pattern of neither the initial flexural cracks nor the shear cracks.

However, the reinforcement type clearly affected the ultimate shear capacity of the deep beams. Although there was no shear reinforcement, the CSA S806 strut and tie model gave a conservative ultimate capacity prediction for the tested deep beams. This shows that the shear reinforcement effect on ultimate shear capacity is not counted in this experiment but it would be recommended only for cracks control.

2.3.2. Shear behavior of slender concrete beams reinforced with BFRP bars. Limited research has been conducted on the behavior of BFRP bars as reinforcement in concrete beams because of the lack of information about their design specifications and construction guidelines. However, many studies were conducted to understand the mechanical characteristics of BFRP bars. These studies show that BFRP bars exhibit higher strength and elasticity and a more effective bond strength with concrete than GFRP bars [19]. Recently, some studies, such as those by El Refaie and Abed in 2016, Issa et al. in 2016 and Alhamad et al. in 2017, have focused on the shear behavior of beams reinforced with BFRP bars. The studies also investigated shear properties such as ultimate loads carrying, modes of failure and crack development. Most of the studies have the same combination of test variables: shear span to depth ratio (a/d), reinforcement ratio and concrete compression strength.

In general, the shear mechanism in beams reinforced with FRP bars is similar to that of beams reinforced with conventional steel except that dowel action within longitudinal reinforcement is ignored in FRP bars, as they are highly dependent on the weak resin. Concrete beams reinforced with FRP bars are weaker in shear than those reinforced with conventional steel with the same reinforcement ratio, test techniques and properties but they still show a comparative shear capacity [20].

A study was conducted to investigate the flexure and shear of concrete beams reinforced with BFRP bars by Tomlinson and Fam in 2014. The beams were reinforced longitudinally with BFRP (6 mm, 8 mm and 10 mm) rebars combined with BFRP

stirrups and steel stirrups and without any shear reinforcement to understand their behavior and failure modes. Nine beams with dimensions of 150×300×3100 mm were tested in four-point bending test to examine the effect of the BRFP longitudinal reinforcement ratio, which varies from 0.28 to 1.60, on the beam performance. The results showed that the ultimate load capacities of the beams are directly dependent on the longitudinal reinforcement ratio regardless of whether the failure mode is flexural failure or shear failure. In the beams tested without stirrups, the load that caused major diagonal cracking was higher for higher BFRP longitudinal reinforcement ratios. On the other hand, the beams reinforced with stirrups all failed in shear by stirrups rapture.

A comparative study, conducted by ElRefai and Abed [17], aimed to understand the shear behavior of concrete beams reinforced with BFRP bars. The experimental program involved 10 rectangular beams reinforced with 8 mm, 10 mm and 12 mm BFRP bars and without transverse reinforcement and 2 beams reinforced longitudinally with conventional 12 mm steel bars. The beams (152 × 254 × 2,000 mm) were tested until. The main test variables were tensile reinforcement ratio ρ, shear span to depth ratio a/d (2.5 and 3.3) and reinforcement type, with a constant concrete compressive strength of 49 MPa. In addition to analyzing the shear behavior, the test results were compared with predictions from various design codes and guidelines, namely CSA 2002, ACI 2015 and JSCE 1997. During the test, many cracks initiated vertically at the bottom of the beams and propagated upward to the concrete compression region. In some beams, horizontal cracks developed towards the supports. All beams failed by diagonal tension cracks.

The results showed that the number of cracks increased as the a/d ratio increase. The large number of observed cracks was attributed mainly to the increase in moment arm due to increase in shear span. The total moment in the constant-moment zone increased with increases in the moment arm. It was observed that, for the same a/d ratio, the cracking load increased linearly as the reinforcement ratio increased. Similarly, the strains in both, the BRRP bars and concrete, were dependent on the reinforcement ratio ρ and increased as the reinforcement ratio decreased. Accordingly, the concrete's contribution to the shear behavior of the beams reinforced with BRPF bars increased as the axial rigidity of the longitudinal bars increased. It also increased as the span to depth ratio decreased. It was concluded that shear strength in beams

reinforced with BFRP bars is proportional to the longitudinal BFRP reinforcement ratio ρ, identical to that of beams reinforced with GFRP and AFRP bars with the same material properties, and significantly less than the shear strength of beams reinforced with CFRP bars.

Another study carried out by Issa et al. aimed to study the shear behavior of concrete beams reinforced with BFRP bars with and without BFRP stirrups. The investigation included twelve (200mm × 300mm × 3050mm) beams in total. Six beams were reinforced in shear and the rest were not. The BFRP flexural reinforcements were 10 mm, 13 mm, 16 mm and 25 mm diameter bars. The main test variables were BFRP reinforcement ratio ρ and shear span to depth ratio a/d. In the beams reinforced without BFRP stirrups, cracks initiated in the constant moment region and were affected neither by the reinforcement ratio ρ nor by the a/d ratios. Furthermore, as the load increased, more flexural cracks initiated in the shear span region. These cracks were more inclined with the presence of shear stirrups. The cracks continued as the beams sustained more load before reaching their maximum load capacity and failing in the shear span region. It was observed that the beams with higher reinforcement ratios sustained a slightly larger number of cracks prior to failure. The governing failure mode was the shear tension mode, observed through the inclined cracks near the supports' edges. According to the ACI-318-14, shear tension failure usually occurs in reinforced concrete deep beams where the a/d ratio is less than 2.5. However; the a/d ratios in the test in beams without shear reinforcement ranged between 5.65 and 7. This can be explained by the fact that BFRP has a lower stiffness compared to conventional steel and hence, when the cracks reached the reinforcement, the BFRP bars started to slip from the concrete.

In addition, a large stress concentration developed due to the high deformation in the BFRP bars that lead to crack formation and a loss of the bond between the BFRP and concrete. It was concluded that as the reinforcement ratio ρ increases, beam stiffness increases significantly and the flexural strain in both, the BRRP bars and concrete, decreases. Some of the beams were reinforced in shear and had a/d ratios of 1.5, making them deep beams. beams recorded a high ultimate load capacity as the reinforcement ratio increased, while the a/d ratios remained constant. This behavior was expected because increases in reinforcement ratio decrease deflection, assuming a constant load. This improves the shear transfer since the crack width and depth is

reduced. The study revealed that BFRP bars are a good alternative reinforcement and that they share theshear characteristics of reinforcement bars with other FRP composites (CFRP, GFRP and AFRP).

In a recent study, Alhamad et al. 2017 [48] studied the effect of shear span to depth ratio on the shear behavior of deep beams reinforced with BFRP. In general, research on the behavior of deep beams reinforced with BFRP is scarce. In this study, a total of four (140 mm×260 mm×2000 mm) beams were reinforced longitudinally with 12 mm BFRP bars without web reinforcement and, one beam was reinforced with conventional steel bars to be used for comparison. The effect of shear span to depth ratio on the shear capacity, load deflection and failure modes was investigated. The results showed that most of the beams failed after the propagation of diagonal shear cracks from the supports to the nearest loading point. One beam that has a 1.5 a/d ratio experienced concrete crushing in compression under the point load linking a diagonal shear crack to the support. A more ductile failure is exhibited in the beam by witnessing crushing in concrete. It was observed that beams reinforced with BFRP bars showed a linear load-deflection relationship unlike the beams reinforced with conventional steel, that exhibited elastic-plastic load deflection until failure. It was concluded that load deflection at any stage increases as the a/d ratio increases. This conclusion can be noticed in beams having large a/d ratios that failed as critical flexural members rather than shear critical ones. The reason for having small deflections in the beams reinforced with conventional steel is that steel bars have a higher post-cracking stiffness than BFRP bars, attributed to the low modulus of elasticity of BFRP bars, which leads to the formation of wide cracks. The strain recorded in the beams reinforced with conventional steel was less than that in the beams reinforced with BFRP in all loading stages of the test. The ultimate shear capacities of the BFRP beams were higher than those of the beams reinforced with steel. Furthermore, a linear inversed curve was observed between the shear strength of the beams and their a/d ratios. For instance, decreasing the a/d ratio in the BFRP beams by 19% (from 1.82 to 1.48) increases the shear capacity by 100% (from approximately 80 to 160 kN). Further reduction in the a/d ratio until 1.15 in the BFRP reinforced beams resulted in an approximately 35% shear capacity increase. Moreover, a linear correlation between shear capacity and cubic a/d ratio was noted and then proved through the Canadian Standards Association CSA S806-12 code [49].

This was attributed to the inclination between the diagonal struts and horizontal ties that resulted in improving the beam arch mechanisms.

2.3.3. Fiber reinforced concrete FRC. Fibers have been consistently used as an advanced construction material to reinforce concrete since the beginning of the 20th century. In general, plain concrete is known for its brittle behavior and low tensile strength, typically around 5-8% of its compressive strength [50]. Consequently, plain concrete is susceptible to the formation of cracks under tensile and compression stresses.

Fibers are frequently mixed with plain concrete to bridge those cracks and arrest their propagation [51]. Many studies focus on the enhancing abilities of fibers in terms of the toughness, ductility and flexural strength of FRC. For instance, steel fibers have a potential to increase the flexural strength of FRC from 30% to 125% that of normal plain concrete depending on the concrete's compressive strength and the fiber dosage [50].

In a comparative study, Reis [52] investigated the mechanical properties of carbon and glass fiber reinforced epoxy polymer concrete (CFRC and GFRC) and compared them with those of conventional plain concrete mixes. The results, summarized in Table 1, revealed that adding fibers to epoxy polymer concrete improves its compressive strength. Specifically, adding carbon-fiber reinforcement resulted in an improvement of 16% in the compressive strength while adding glass-fiber reinforcement resulted in an improvement of only 8.7%.

The behavior was different when the elastic modulus was analyzed. Both the carbon and glass fibers had no significant impact on the compression modulus of elasticity. In comparison with beams of market normal concrete mixes, plain epoxy concrete beams showed a higher compressive strength by 17.3% to 33.7% [52].

Glass fiber reinforced epoxy polymer concrete showed slightly higher compressive strengths with values higher than those of market concrete mixes by 27.5% to 45.4 %. The carbon-fiber reinforced epoxy polymer concrete specimens displayed much higher compressive strengths with values 36.1% to 55.1% higher than those of normal concrete. Poisson's ratio showed no significant effect on compressive strength [52].

Table 1: Comparison between plain concrete and (Glass and Carbon) FRC [42].

Test Series	Compressive Properties (Average)		
	Strength (Mpa)	Elastic Modulus (GPa)	Poisson's Ratio
Plain	59.681	11.281	0.259
CFRC	69.215	10.882	0.247
GFRC	64.873	11.551	0.257

A more recent study conducted by Branston et al. [53] aimed to evaluate the effectiveness of Basalt fiber in improving the mechanical behavior of concrete beams in terms of flexural behavior. The test mainly focused on comparing the pre and post-cracking behavior of concrete beams. Beams were cast with two types of Basalt fibers (chopped and minibars) and with the commonly-used hooked-end steel fiber, with three different quantities of each fiber type. The results showed that beams reinforced with chopped Basalt fibers have better first crack strength resistance under flexural loading. This strength resistance increases dramatically with increases in fiber dosage and length. In contrast, the addition of chopped basalt fibers showed no significant effect on the post-cracking behavior of the concrete beams. This was attributed to the poor cracking response caused by rapture failure in the chopped fibers. The test illustrated that a dosage of 12 kg/m^3 of 50 mm chopped Basalt fiber can be considered equivalent to a dosage of 40 kg/m^3 of steel fiber. The same effect on first crack strength was observed with the addition of minibars Basalt fibers.

However, minibars fibers had a strong positive impact on post-cracking strength resistance. An addition of 20 kg/m^3 of minibars increased both pre and post cracking strength by a percentage comparable with the addition of 40 kg/m^3 of steel fibers under flexural behavior.This ability of minibars was attributed to the pull-out failure mode of beams reinforced with minibars fibers that was clearly observed in through their ductile behavior. On the other hand, the results showed that the addition of both chopped and minibars fibers simultaneously would not be an effective way to increase compressive strength. It is important to ensure that adding fibers to concrete does not affect its workability or compressive by choosing an appropriate dosage of fibers. Figure 5 shows the load-deflection results of the specimens. As illustrated by the plots in Figure 5.

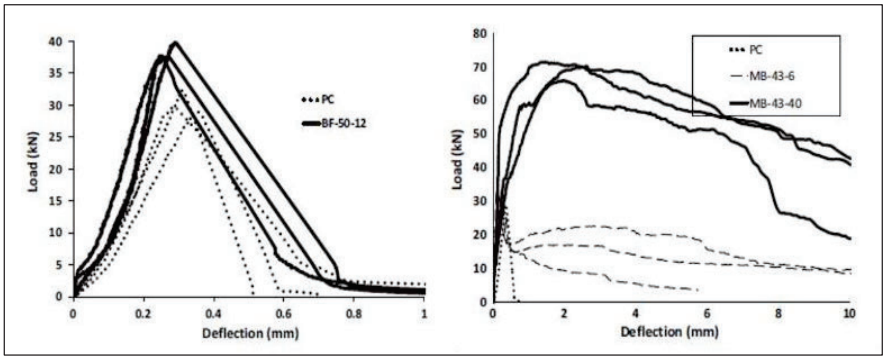

Figure 5: Load-Deflection results for specimens reinforced with (Bundled fibers Vs Minibar fibers) [43]

A recent comparative study conducted by Simeos et al. [50] focused on the mechanical behavior of fiber-reinforced concrete. The study included three hundred and twelve specimens containing three types of fibers as reinforcement, namely polypropylene, glass and steel fibers. mixture. The study targeted the compressive strength, cracking load, maximum load, ductility, and bending behavior of the mixes. The results showed that the compressive strength tends to increase with the addition of fibers. The confinement of the fibers has the main role in enhancing the compressive strength of the mixture, where the enhancement increases with fibers' resistance to poisson's ratio effect. Thus, the compressive strength is higher in the mixtures containing fibers of higher stiffness and tensile strength.

Accordingly, compared to the reference mix, the compressive strength of the polypropylene and glass reinforced mixes was lower while that of the steel fiber reinforced mix was higher. In terms of the load deflection behavior, ductile behavior is witnessed in mixes containing ductile fibers. Fatigue was observed in the polypropylene and steel fiber reinforced mixes and fragility was observed in the glass fiber mix. In comparison to the reference plain concrete, the maximum load resistance increased with fiber addition.

The load resistance capacity was higher in mixtures containing fibers of higher tensile strength. Accordingly, the lowest load resistance was observed in the polypropylene mix and the highest in the steel fiber mix. Although the glass fiber mix's toughness was not determined due to its fragility, the toughness of the steel and polypropylene concrete mixes increased with increases in the amount of added fiber.

Chapter 3. Experimental Program

In this chapter, the material properties, the specifications of test specimens, the test equipment, the test setup, and the procedure are presented.

3.1. Materials Properties

A concrete mix containing basalt microfibers is created. Beams were casted from this mix and reinforced with BFRP bars. Another mix is created with synthetic microfibers. Beams were casted from this second mix and similarly reinforced. The beams from the two different mixes are then compared to each other. The used materials are basalt microfibers, synthetic microfiber, BFRP bars of (10, 12 and 16) mm diameter and concrete mixes of 45 and 60 MPa compressive strengths.

3.1.1. Concrete mix. The tested beams are cast using a normal weight concrete mix of a 2484 kg/m^3 unit weight. The dosage of basalt microfibers is 0.75 % per mix volume. The basalt fiber reinforced concrete (BFRC), synthetic fiber reinforced concrete (SFRC) and normal reinforced concrete (NRC) mixes have an average 28-day targeted compressive strength of 45, while high strength basalt fiber reinforced concrete (HBFRC) has 60 MPa compressive strength. Concrete cylinders, cubes and beams specimens are tested under compression in order to evaluate the exact concrete compressive strength (f'c), and tensile strength. Additionally, the effect of adding microfibers in concrete mix is investigated by creating cubes, cylinders and small beams specimens without fibers and compare the results with specimens containing fibers. Many previous studies have indicated that adding microfibers to a concrete mix will result in increasing the compressive strength of beams cast from that mix [44,45]. Table 2 shows the different concrete mixes design that used in the study.

Table 2: Concrete mix design

Concrete Mix	Fiber Content (kg/m3)	Unite Weight (kg/m3)							
		Cement	Microsilica	Water	Aggr. (20 mm)	Aggr. (10 mm)	Washed Sand	Dune Sand	PCE superplasticizer
BFRC-45	19.5	390	-	148	640	320	636	321	26
SFRC-45	1.8								
FRC-45	-								
HBFRC-60	19.5	440	20	138	650	360	600	220	29.4

3.1.2. Basalt fiber-reinforced polymer bars (BFRP). BFRP bars of 3 different diameters are used as longitudinal reinforcement. Each tested beam contains two longitudinal BFRP bars of same diameter. Figure 6 shows the different BFRP bars of 10 mm, 12 mm, and 16 mm diameter. The outer surface of the BFRP bars is coated with sand. To obtain the actual values of tensile strength and modulus of elasticity of the BFRP bars, a sample of used bars is tested in the lab. According to a tensile test conducted on same BFRP bars, the tensile test results are summarized in Table 3.

Table 3: Tensile Test Results

Bar Type	Cross sectional area (mm^2)	Ultimate Tensile Stress (MPa)	Ɛu: Ultimate strain %	E: Modulus of elasticity (GPa)
BFRP10	78.5	1227±55	2.7±0.1	46.1±1.1
BFRP12	113.1	1230±80	2.7±0.2	46.3±0.4
BFRP16	201.1	1177.3±56	2.7±0.2	46±2.1

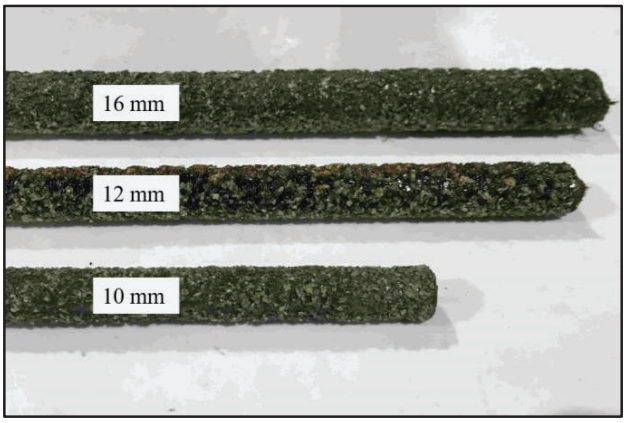

Figure 6: BFRP bars of different diameters.

3.1.3. Synthetic fibers. Synthetic microfibers are used as a test parameter in the tested short beams. The shear capacity of these beams is compared with that of the beams reinforced with basalt microfibers. Synthetic microfibers have a tensile strength of 650 MPa and an elastic modulus of 2.5 GPa [56]. Synthetic microfibers are integrated in the concrete mix in this study and their effect on shear response of BFRP-FRC beams is investigated. Figure 7 shows a synthetic microfiber sample that used in the study

[57]. Table 4 summarizes the mechanical properties of the used synthetic microfibers as per the manufacturer.

Figure 7: Sample of Synthetic fibers.

Table 4: Synthetic fibers mechanical properties

Type of fiber	Standard Length (mm)	Specific Gravity	Young's modulus (GPa)	Tensile Strength MPa
Synthetic	12	0.92	2.5	650

3.1.4. Basalt fibers. In this research, Basalt microfibers will be used in the concrete mix of BFRP short beams. Basalt microfibers have an average tensile strength of 924.3 MPa and an elastic modulus of 61.8 GPa [58]. Basalt microfibers are integrated into BFRP short beams to investigate their role in prohibiting the development of micro cracks and reducing crack width. Figure 8 shows a sample of basalt microfibers that integrated into the concrete mix that used in the study [53]. Table 5 sum up the mechanical properties of the used basalt fibers as per the manufacturer.

Figure 8: Sample of Basalt fibers [43].

Table 5: Basalt fibers mechanical properties

Type of fiber	Standard Length (mm)	Specific Gravity	Young's modulus (GPa)	Tensile Strength (MPa)
Basalt	24	2.6	61.8	924.3

3.2. Four-Point Bending Test

In the experimental work, eight short beams are prepared for testing as presented in Table 6. The experimental program is mainly performed using the four-point bending test to investigate the effect of different types of microfibers on the shear response of BFRP-reinforced short beams. All beams are reinforced longitudinally without web reinforcement. Also, all beams have constant cross section of 150 mm width, 260 mm depth and 2000 mm span length. As previously mentioned, the test variables in this research are the fiber types, the span-to-depth-ratio (a/d), longitudinal reinforcement ratios (ρ) and the concrete compressive strength(f'_c). The shear response of the tested beams is studied using tension reinforcement of (No.10, 12, 16 mm) BFRP bars. A total number of six beams are casted using concrete mix containing basalt fibers, one beam is casted from a concrete mix containing synthetic microfibers and one beam casted using plain concrete mix for comparison purposes. The effect of using different shear span-to depth ratio is examined using three different (a/d) values of 1.15, 1.48 and 1.82. The effect of reinforcement ratio is evaluated using three different ρ values of 0.49, 0.70 and 1.26.

The beams are designated based on fiber type that used in concrete mixes and concrete mix compressive strength followed by the number of longitudinal rebars and the value of shear span-to-depth ratio. A labeling system is implemented for the specimens where the first letter (B, S or P) indicates the type of the fibers that used in the concrete mix where B refers to basalt-fiber containing, S for synthetic-fiber containing and P for plain concrete mix. Then the letter N or H indicates the concrete compressive strength which N is normal concrete mix of 45 MPa and H is high strength concrete with 60 MPa. The next number refers to the number of rebars used followed by T that specifies the diameter of BFRP bars in millimeter. The last number indicates

the different shear span to depth ratios. For instance, BN2T10_1.15 indicates the beam that contains basalt fibers in a normal compressive strength concrete mix and reinforced with two bars No.10 with 1.15 shear span to depth ratio. The beam specimens, their labels, and their specifications are listed in Table 6.

Table 6: Details of test specimens

Sr#	Beam	A (mm^2)	ρ %	a/d	Types of fibers	f'_c (MPa)
1	BN2T10_1.15	2#10 = 157	0.49	1.15	Basalt Fiber	45
2	BN2T12_1.15	2#12 = 226	0.70	1.15	Basalt Fiber	45
3	BN2T16_1.15	2#16 = 402	1.26	1.15	Basalt Fiber	45
4	BN2T12_1.48	2#12 = 226	0.70	1.48	Basalt Fiber	45
5	BN2T12_1.82	2#12 = 226	0.70	1.82	Basalt Fiber	45
6	BH2T10_1.15	2#10 = 157	0.49	1.15	Basalt Fiber	60
7	PN2T10_1.15	2#10 = 157	0.49	1.15	None	45
8	SN2T10_1.15	2#10 = 157	0.70	1.15	Synthetic Fiber	45

The tested beams were divided into four main sets to investigate the effect of each test parameter on load-deflection relationships, mode of failures and shear strength of the studied beams. The first group (BN2T10_1.15, PN2T10_1.15 and SN2T10_1.15) was utilized to study the influence of using basalt and synthetic fibers on the shear response of the tested beams. The second set (BN2T12_1.15, BN2T12_1.48 and BN2T12_1.82) was used to investigate the effect of different shear span to depth ratios (a/d). The third group (BN2T10_1.15, BN2T12_1.15 and BN2T16_1.15) was developed to examine the effect of using different reinforcement ratios (ρ). The remaining set (BN2T10_1.15 and BH2T10_1.15) was aimed to study the effect of concrete compressive strength (f'_C). Figure 9 shows the cross section of the test beams.

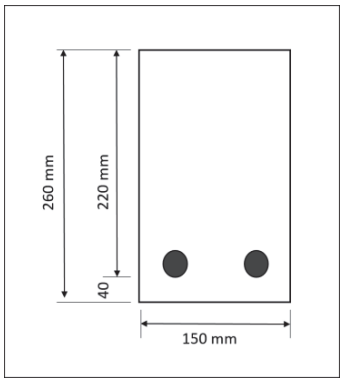

Figure 9: Beam cross-section

3.2.1. Test setup and instrumentation. The beams are tested using four-point bending test over a simply supported span of 1000 mm to determine the different shear capacities. Each beam is loaded at four points; two points work as support points and the other two points are carry the actual load on the beam outer surface. The load is applied in a way that the span between the loading points has zero shear, while the span between each support point and the nearest loading point, known as the shear span, has the maximum constant shear. A high accuracy linear variable displacement transducer (LVDT) instrument is installed at the beam's mid-span to measure its deflection with increasing load. As mentioned, the clear span of tested beams is 1000 mm, with 500 mm overhang on each end side to provide sufficient development length for the reinforcement bars. The test and instruments setup are shown in Figure 10.

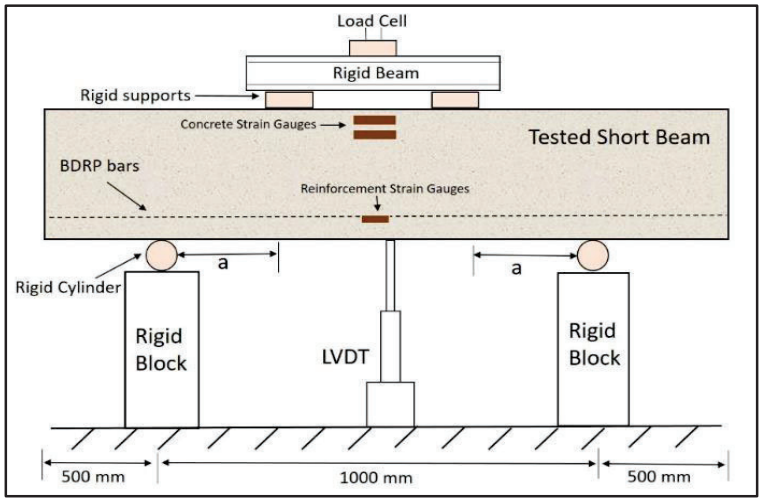

Figure 10: Test instrumentation and specimen setup

Moreover, strain gauges are used to measure the strain in the reinforcement bars and the top concrete fibers. The applied load, displacements and strain readings are electronically recorded during the test using data acquisition system monitored by a computer. The load on the beams is applied using the universal testing machine (UTM) with a maximum load capacity of 2500 kN as shown in Figure 11.

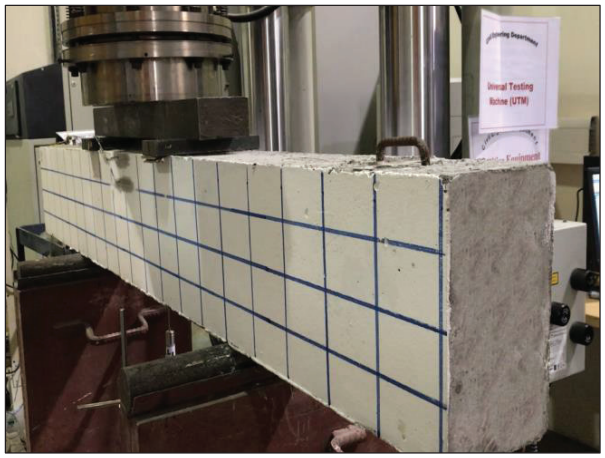

Figure 11: Universal testing machine (UTM)

3.3. Strut and Tie Method

The strut-and-tie modeling (STM) method has been established since the infancy of reinforced concrete design. Back in 1899, Wilhelm Ritter developed the truss mechanism in concrete beams to explain the contribution of transverse reinforcement bars to the shear capacity of concrete beam [59]. In the late 19 century, an increased interest in STM based on complex load analysis had begun to appear. Marti and Schalaich et al. presented the STM approach to be used in the discontinuity regions in concrete beams where shear stresses and deformations are the dominant influence [59].

Following this presentation, the STM started to appear in North American codes in general design provisions. In 1984, the Canadian code CSA A23.3 became the first code to adopt the STM [60]. Afterwards, the STM was adopted by AASHTO for segmental guide specifications specifically in 1989 [59]. Recently, the American Concrete Institute (ACI) introduced STM provisions, specifically in the 2002 edition of the Building Code Requirements for Structural Concrete [61].

In any concrete beam, two types of regions can be defined: B-regions, short for "beam regions," and D-regions, short for "distributed regions" [62]. Various types of D-regions are shown in Figure 12. Normal sectional analysis procedures are usually considered appropriate for designing B-regions in which the longitudinal strain has a generally linear variation over the depth of the beam [62]. On the other hand, D-regions have a nonlinear strain distribution due to the presence of concentrated loads, geometrical changes, or discontinuities [43].

Therefore, in those regions, the strains due to shear forces are significant and the design method should consider the non-linear distribution of the stress field. In this situation, it is not correct to assume that a beam's cross section remains plane or that the shear stresses are uniform [62]. These D-regions require a method of analysis that considers those complexities [62].

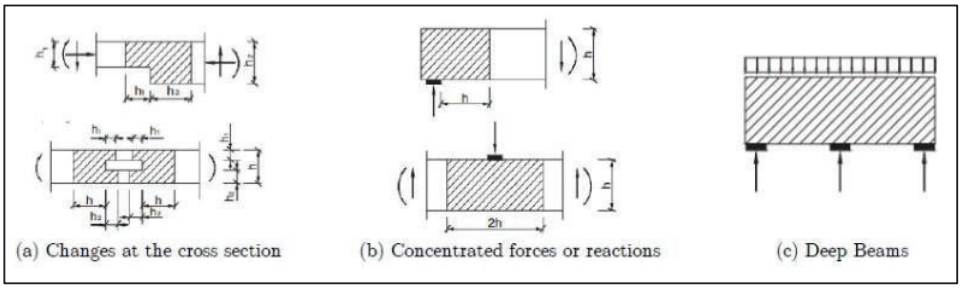

Figure 12: Examples of D-regions [51]

The strut-and-tie method is an analytical approach that has been proven to provide a valid analysis and design of those D-regions in concrete beams. The STM method idealizes the complex flow of stresses in these regions by establishing a hypothetical pin-joined truss model through the beam in which compressive members are referred to as "struts" and tensile members are referred to as "ties" [63].

Struts and ties are connected at nodes. The node in an STM model is a point in a joint where struts, ties and concentrated loads are connected. Figure 13 shows a typical short beam and its STM model. Figure 13 also shows that the beam is tested using the four-point load test in which two points are loaded on the top face of the beam and two points are supported on the opposite face.

The main longitudinal reinforcements are located at a distance d from the top of the beam[64]. The hypothetical truss that used in this research is consisted of two diagonal struts, upper horizontal strut and one lower horizontal tie. Those struts members are connected at two nodal zones and two reaction joints.

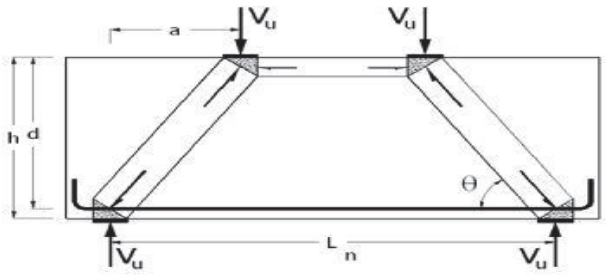

Figure 13: Geometric of short beam with STM model [53].

The process of designing a strut-and-tie model to sustain the imposed forces acting on D-regions includes the following steps as assigned by the ACI-318-14 code [43]:

- Designate and isolate each D-region separately.
- Calculate the total resultant forces acting on each D-region boundary.
- Compute the forces acting on the struts and ties of the model in order to transfer the resultant forces across the whole D-region.
- Design the struts, ties, and the nodal zones such that they end up with sufficient strength. By considering the concrete strength, the width of the struts and ties can be determined.
- The design of the strength capacity of a strut, tie or nodal zone (ΦF_n) must be larger or at least equal to the force in the strut, tie, or nodal zone. According to ACI-318-14 suggested the strength reduction factor $\Phi = 0.75$

$$\Phi F_n \geq F_u \quad (1)$$

The following equations are ACI-318-14 requirements for strut and tie design:

A- Strength of diagonal and horizontal struts:

The nominal compressive strength of a strut that does not contain longitudinal reinforcement is taken as

$$F_{ns} = f_{ce} A_{cs} \quad (2)$$

Where A_{cs} is the area of the beam cross section at one end of the strut, taken perpendicular to the axis and f_{ce} is the effective compressive strength of the concrete in the strut and the nodal zone. Its value to be taken is the lesser of the following two criteria:

(a) Effective concrete compression strength in struts

$$F_{ce} = 0.85\,\beta_s f'_c \qquad (3)$$

Where β_s refers to the factor used to estimate the effect of both, cracks and the confinement of the reinforcement, on the strength of the strut concrete. The value of β_s is given in the ACI code in appendix section A.3.2 and it varies from 0.4 to 0.75.

(b) The nominal compression strength of a nodal zone, F_{nn}

$$F_{nn} = f_{ce} A_{nz} \qquad (4)$$

Where A_{nz} is the smaller of the following two values:

- The area of the face of the nodal zone where F_u acts, taken perpendicular to the line of action of F_u.
- The area of a section through the nodal zone itself, taken perpendicular to the line of action of F_u.

The effective concrete compression strength in nodal zones is given by the following equation

$$F_{ce} = 0.85\,\beta_n\,\mathrm{f'c} \qquad (5)$$

Where β_n is the factor used to estimate the effect of the anchorage of ties on the effective compressive strength of the nodal zone. Its values are listed in ACI appendix A.5.2 for different situations and generally vary from 0.6 to 1.0, depending on the number of ties and bounds of the nodal zone.

B- Strength of the horizontal tie:

In accordance with the ACI 318 specifications, the nominal strength of the tie is calculated as the final sum of yield strength of the conventional steel reinforcement plus the forces in the prestressing steel. The last term is considered as zero if there is no prestressing steel used in the tie. The general strength of the tie is given as following

$$F_{nt} = A_{ts} f_y + A_{tp}(f_{se} + \Delta f_p) \quad (6)$$

Where

A_{ts}= Area of nonprestressed reinforcement in tie.

f_y = Yield strength of the nonprestressed reinforcement.

A_{tp}= Area of the pre-stressed steel in the tie.

f_{se}= Effective stress in the pre-stressed reinforcement after losses.

Δf_p= Increase in stress in the pr-estressed steel due to factored loads.

(f_{se}+Δf_p) shall not exceed f_{py}.

C- Strength of Nodal Zones

The nominal compressive forces at any face of the two nodal zones that generated by the act of diagonal and horizontal forces is given by:

$$F_{nn} = f_{ce} A_{nz} \quad (7)$$

Where A_{nz} refers to the area of a section through the nodal zone itself, taken perpendicular to the strut axis. The effective concrete compression strength in nodal zones is given by the following equation

$$F_{ce} = 0.85\, \beta_n\, \mathrm{f'c} \quad (8)$$

Where β_n is the factor used to estimate the effect of the anchorage of ties on the effective compressive strength of the nodal zone. Its values are listed in ACI appendix A.5.2 for different situations and generally vary from 0.6 to 1.0, depending on the number of ties and bounds of the nodal zone.

Chapter 4. Results

4.1. Material Evaluation

Four different mixes are used in this research: normal plain reinforced concrete (NRC), normal basalt fiber reinforced concrete (BFRC), normal synthetic fiber reinforced concrete (SFRC), and high strength basalt fiber reinforced concrete (HBFRC). The concrete compressive strength (f'_c), concrete modulus of elasticity (E) and concrete tensile strength are obtained for all types of concrete mixes using compression and split tensile tests. The results of compression and split tensile tests were utilized to evaluate the strength of all concrete mixes and investigate the main influence of basalt and synthetic microfibers on concrete mechanical properties.

All concrete beams and small specimens were prepared and cast with two main strength targets: a normal concrete mix (45 MPa) and high strength concrete (60 MPa). The study beams and small specimens of cubes (150 x 150 mm), cylinders (150 x 300 mm) and beams (100 x 100 x 500 mm) are cast in the concrete factory, and demolded from formworks and molds after 48 hours as shown in Figure 14.

After that, all beams were covered by cloth sheets and cured with water for one week. Likewise, concrete cubes, cylinders and beams specimens are cured in university labs by being kept in water tanks for 28 days at same curing conditions. After curing period, concrete cylinders and cubes are tested using compression and split tensile tests in order to obtain the actual compressive strength of concrete mixes. Figure 14 shows the cast and curing processes of study beams and specimens.

(a) (b) (c)

Figure 14: (a) Concrete formworks (b) Concrete curing process (c): Specimens casting process.

4.1.1. Compressive strength. After performing concrete compressive strength test according to ASTM C109/C109M [65], the presence of microfibers in concrete design relatively enhanced the mechanical properties of concrete mixes. The summarized results in Table 7 and Figure 16 indicate that, cubes contain basalt microfibers have yielded by an average compressive strength of 50.98 MPa and improved the compressive strength of concrete mix by 6.82% in comparing with plain concrete mix.

On the other hand, cubes containing synthetic microfibers resisting an average compression strength of 48.33 MPa and increase the compressive strength of concrete by 1.72% only. Furthermore, it was noticed that the failure mode of the cubes is influenced by contribution of microfibers in concrete mixes, since that the basalt and synthetic microfibers bridging the micro cracks in concrete cubes which exhibited a less destructive failure modes as shown in Figure 15.

(a) NRC (b) BFRC (c) SFRC

Figure 15: Concrete cubes failure modes: (a) NRC, (b) BFRC, (c) SFRC

Table 7: Mechanical properties of concrete mixes

Concrete Type	Sample	Compressive Strength, (f'_c)	Average Compressive Strength (MPa)	Modulus of Elasticity (GPa)
NRC	1	48	47.5	26.36
	2	47		
BFRC	1	46	50.98	29.17
	2	54		
	3	53		
SFRC	1	47	48.33	28.22
	2	49		
	3	49		
HBFRC	1	58	57.5	29.93
	2	57		

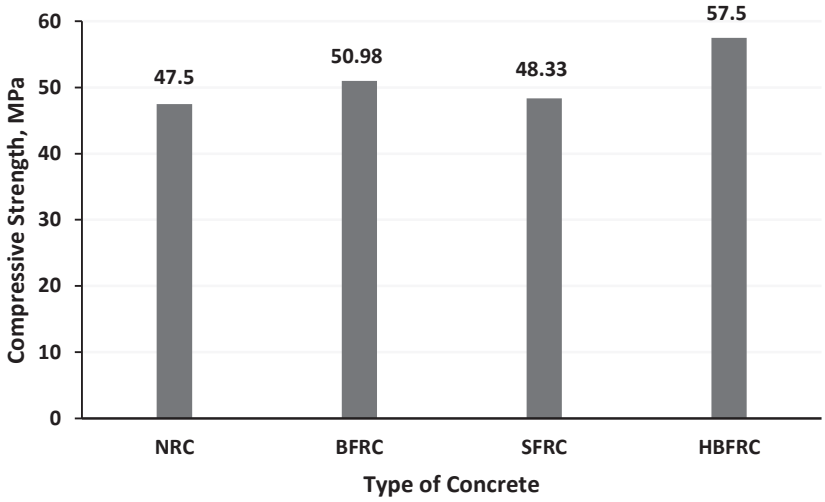

Figure 16: Average compressive strength of different concrete mixes

4.1.2. Split tensile. The tensile strengths of concrete mixes that contain fiber are obtained experimentally using three cylinders for each mix. The test is carried out on (150 * 300) cylinders using compression test machine by splitting along their middle plane and parallel to the edge in accordance to ASTM C469[66]. The split tensile strength of concrete cylinders is calculated using equation 9, test results are summarized in Table 8:

$$\sigma_t = \frac{2P}{\pi LD} \tag{9}$$

Where, P is the compressive load at failure, N

L = length of the cylinder, mm

D = diameter of the cylinder, mm

Table 8: Split Tensile Strength

Type of fiber	Maximum Load (kN)	Split Tensile (MPa)
Basalt	266.48	3.77
Synthetic	218.96	3.11

4.1.3. Flexural strength. For each concrete mix, two small beams were casted to perform flexural tensile strength using four-point loading test according to the ASTM C1609/C1069M standard[65]. The unreinforced concrete beams have standard dimensions of (100 x 100 x 500 mm). Two equal point loads are applied by flexural test machine with loading rate of 0.100 mm/min at a distance of one-third from beam supports (100 mm), so beams are subjected to pure bending in its clear span. a typical arrangement of the flexural strength test is illustrated in Figure 17.

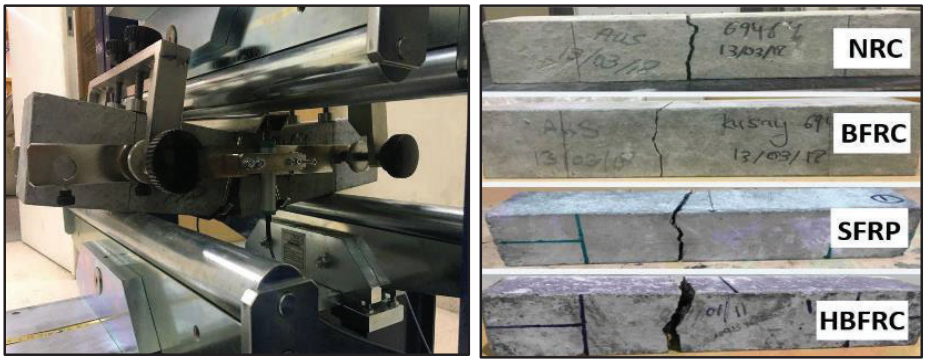

(a) (b)

Figure 17: (a) Flexural strength test (b) small beams specimens

The maximum load at failure was obtained to calculate the modulus of rapture for all beams specimens using the following ASTM C1609/C1069M[67] equation:

$$R = \frac{PL}{bd^2} \qquad (10)$$

Where, R is the modulus of rapture, MPa

P = Maximum vertical load, N

L = Beam span length, mm

b = The width of specimen, mm

d = The height of specimen, mm

After applying equation 10 to all mixes, the following Table 9 summarizes rapture strength for all types of concrete and Figure 18 illustrates the deflection of all small beams. From results, it is obvious that addition of microfibers in concrete mix increased the required force to initiate first crack in concrete beams and hence raised its modulus of rapture value. In addition, it is known that concrete generally fails in

brittle manner when it reached its modulus of rapture. From Figure 18, it was noticed that the existence of basalt and synthetic fibers have increased concrete ductility this agrees with initial expectations about adding fibers to concrete mix.

Table 9: Flexural Strength Test and Modulus of Rapture

Concrete Type	Load (kN)	Modulus of Rapture (MPa)
NRC	16.21	4.86
BFRC	18.07	5.42
SFRC	16.18	4.85
HBFRC	19.79	5.93

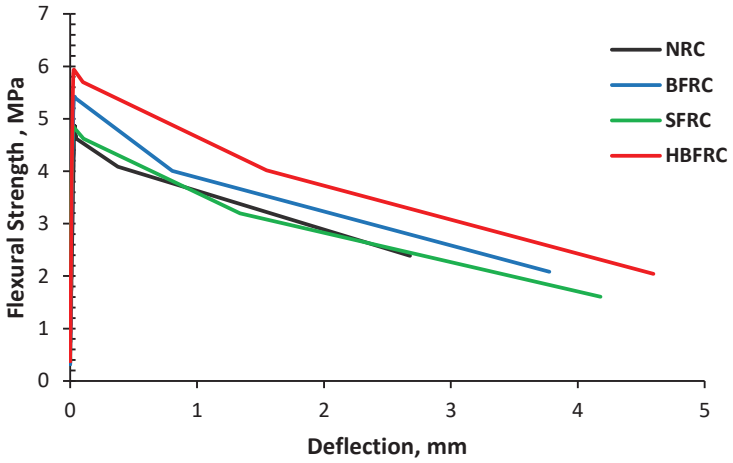

Figure 18: Modulus of rapture vs. deflection of all beams

4.2. Beams Results

The results of all beams were grouped in four different graphs based on the research variables. First group combines RC beams with different fiber types of basalt, synthetic and plain (Group 1). The second group relates three BFRC-FRC beams with different shear span-to-depth ratios 1.15, 1.48 and 1.82 (Group 2). Third graph illustrate the effect of different reinforcement ratios 0.49, 0.70 and 1.26 (Group 3) on BFRC-FRC short beams. The last group demonstrates BFRC-FRC short beams with 45 and 60 MPa compressive strengths (Group 4).

4.2.1. Load vs mid-span deflection. The load verses mid-span deflection curves for all groups are plotted as shown in Figure 19. The first graph targets the effect of basalt microfibers, second graphs related to using different a/d ratios, third graph illustrates the effect of using different ρ and last graphs shows the effect of using high strength concrete. In addition, the crack pattern and failure modes of all beams are demonstrated and summarized in Table 10 and Figure 20.

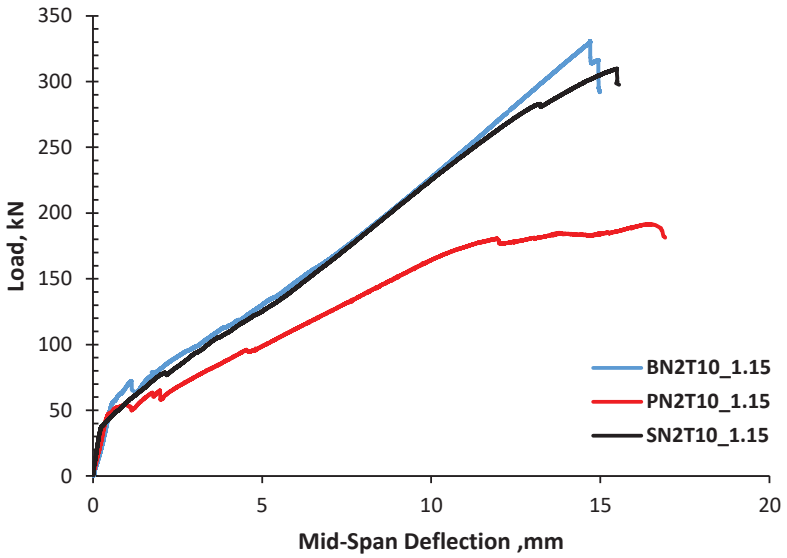

(a)

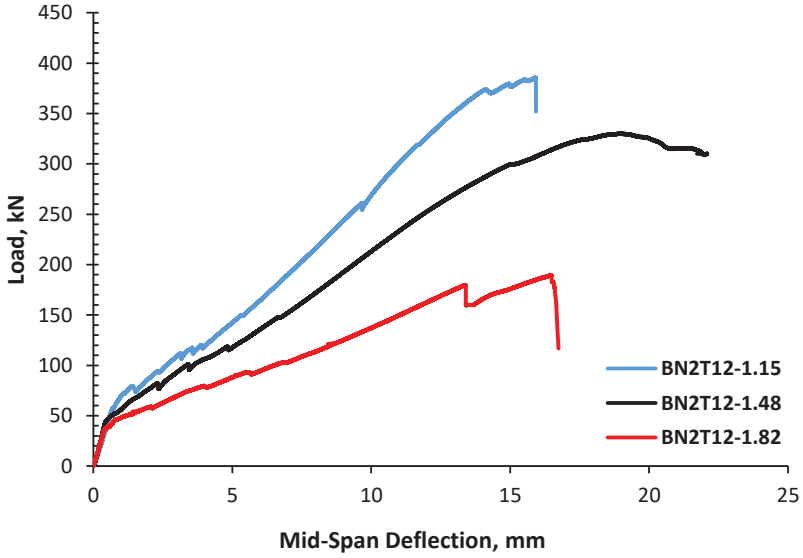

(b)

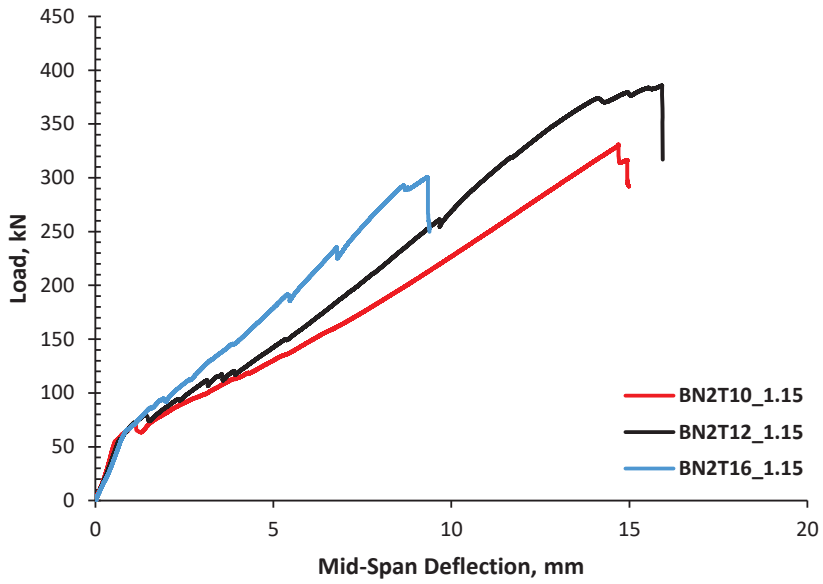

(c)

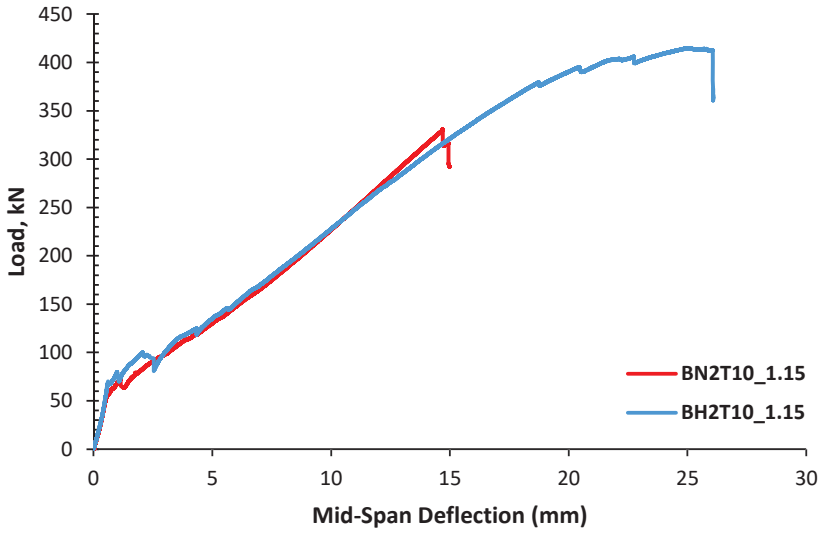

(d)

Figure 19: Load vs Mid-span deflection for tested beams: (a) different fiber types; (b) different shear span to depth ratios; (c) different reinforcement ratios; (d) different concrete compressive strength.

4.2.2. Crack behavior and failure modes. In this research, all eight beams exhibited an ideal shear failure, which was expected due the absence of the shear reinforcement. This was intentionally predesigned for all beams in order to investigate the effect of basalt microfibers in enhancing the shear capacity of short beams. Figure

20 shows the crack patterns of tested beams at ultimate load. Three beams showed a shear failure by developing a major diagonal crack extending from the loading point to the support, followed by splitting in BFRP bars and concrete crushing in the diagonal struts. Four other beams were failed by diagonal shear cracks followed by splitting only between BFRP bars and concrete at maximum load. Only one beam out of the eight was failed by splitting and crushing in the top concrete.

The dominant failure mode in the tested beams was found to be splitting between BFRF bars and concrete after the widening of the diagonal shear cracks that propagate from the loading points to the beam supports. All tested beams in the four groups are compared to each other based on the different research variables and discussed in the next chapter. Beams' maximum load capacity, maximum mid-span deflection and failure modes are summarized in Table 10.

Table 10: Ultimate Shear Capacity of Experimental Work

Sr#	Beam	Failure Load P_{exp} (kN)	Max Mid-Span deflection (mm)	Failure Mode
1	BN2T10_1.15	330.82	15	Splitting
2	BN2T12_1.15	385.79	18.03	Splitting and concrete crushing in diagonal strut
3	BN2T16_1.15	300.44	9.32	Splitting
4	BN2T12_1.48	330.15	22.28	Splitting and concrete crushing in diagonal strut
5	BN2T12_1.82	189.39	17.75	Splitting and concrete crushing in top concrete
6	BH2T10_1.15	414.88	26.08	Splitting and concrete crushing in diagonal strut
7	PN2T10_1.15	191.51	16.46	Splitting
8	SN2T10_1.15	309.79	15.55	Splitting

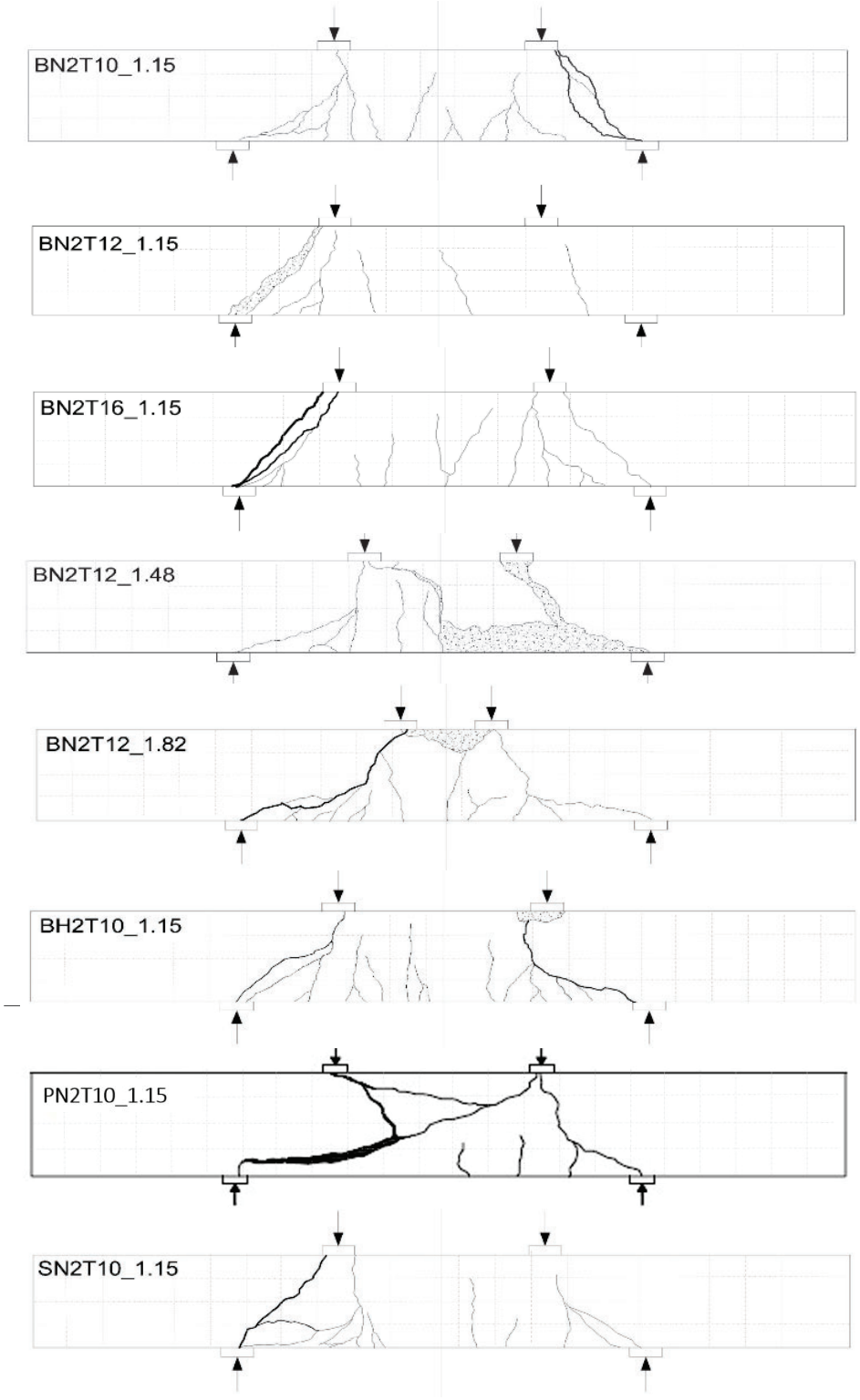

Figure 20: Crack patterns at the ultimate load

4.2.3. Strain at the top concrete and longitudinal bars. The strain values of concrete at the top fibers of the short beams and at the BFRP longitudinal reinforcement were measured using accurate data acquisition system by fixing strain gauges at the mid-span of the concrete and reinforcement bars. Table 11 shows the concrete and reinforcement strains of tested beams at ultimate load. Furthermore, Figure 21 demonstrates the load verses strain values of the BFRP-FRC concrete beams at a 10 mm distance from the extreme compression edge of the short beams and for BFRP reinforcement bars.

Table 11: Concrete and reinforcement strain at ultimate load

Beam	Concrete Strain	Reinforcement Strain
BN2T10_1.15	0.000181	0.021796
BN2T12_1.15	0.001274	0.013563
BN2T16_1.15	0.001242	0.009793
BN2T12_1.48	0.002098	0.021550
BN2T12_1.82	0.002819	0.015640
BH2T10_1.15	0.001773	0.035567
PN2T10_1.15	0.000387	0.015726
SN2T10_1.15	0.000058	0.0181305

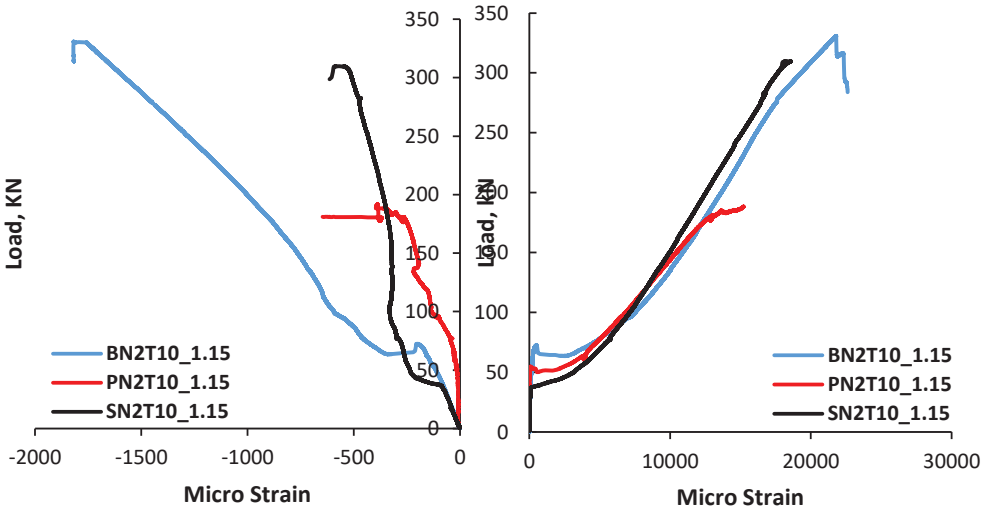

(a)

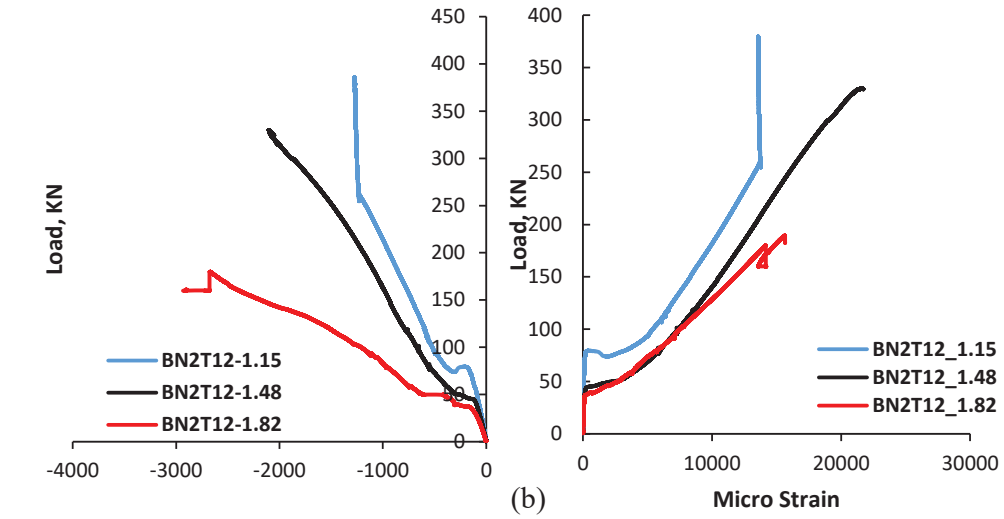

(b)

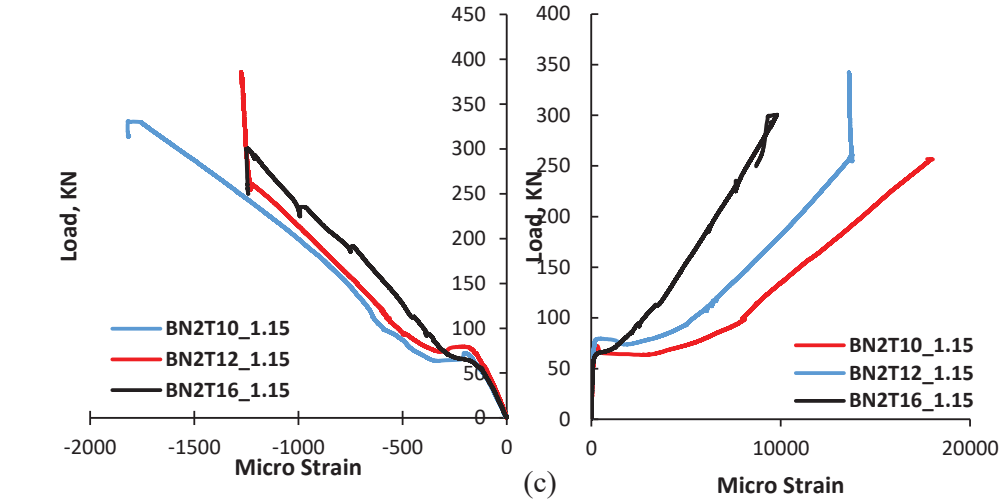

(c)

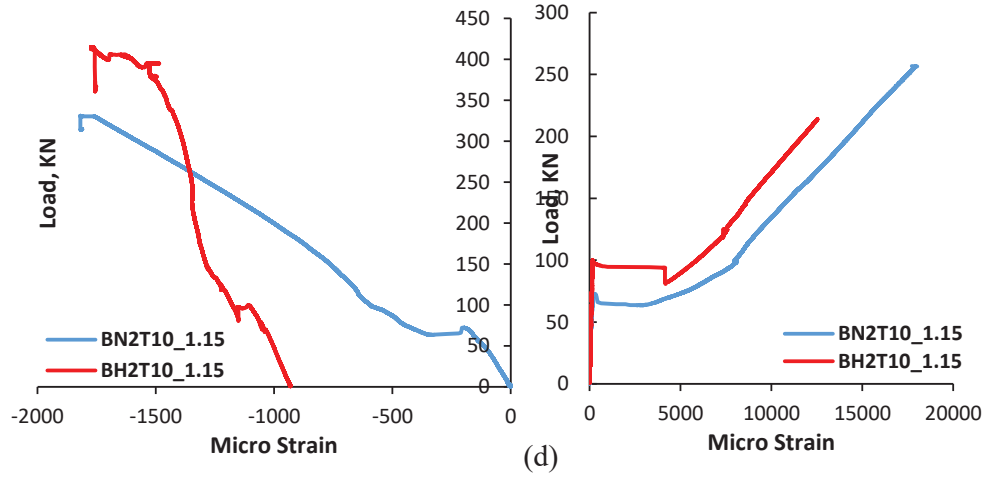

(d)

Figure 21: Load vs concrete and Reinforcement Strain for: (a) different fiber types; (b) different shear span to depth ratios; (c) different reinforcement ratios; (d) different concrete compressive strength.

4.3. Shear capacity using strut and tie method

The proposed strut and tie method that represented in Figure 22 is a hypothetical truss that consisted of: (a) horizontal tie at a depth, d, located from the concrete compressive fibers, (b) a bottled-shape diagonal strut with W_s thickness and (c) a horizontal strut located at the top of concrete fibers with h_s thickness. The following equations gave an example of the followed procedure of STM according to the ACI-318-14 provisions for beam BN2T10_1.15.

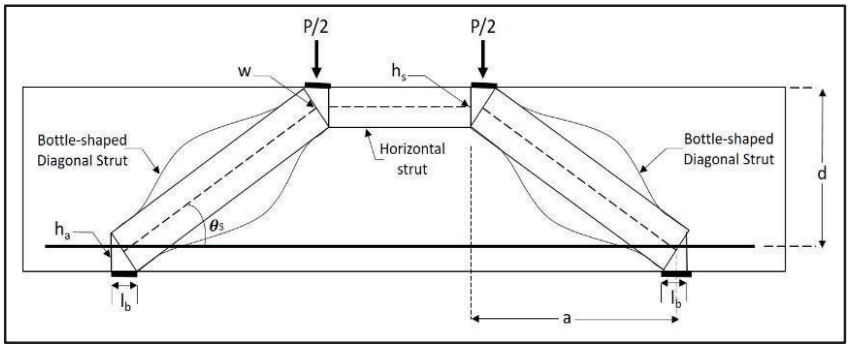

Figure 22: Description of the proposed strut and tie model

Beam BN2T10_1.15 was proposed as an example in applying the strut and tie provisions according to ACI-318-14 in the tested beams. After applying the STM provision on beam BN2T10_1.15 givens, the satisfying optimal ultimate shear strength is found to be 236 kN with 118 kN on each loading points. This value was obtained by iterating the horizontal strut thickness h_s in order to maximize the calculated shear capacity of the beam. The smaller the depth of $h_s$the larger was the angle θ_s and hence resulted in higher forces that should be resisted by truss elements. The obtained theoretical ultimate shear strength was proven to ensure safe forces capacity of strut, tie and nodal zones according to STM method in ACI-318-14 code. STM method is represented by its depth, d, as well as shear span-to-depth ratio, a/d, which considered as the dominant factor that governed the STM method rather than the reinforcement ratio, that was not provided in ACI-318-14 STM provisions.

A- Checking the strengths of diagonal and horizontal struts.

This step aims to examine the ability of the diagonal and horizontal struts to resists the generated forces that resulted from the obtained ultimate applied load by

comparing the actual load forces generated in diagonal and horizontal struts, F_{ds} and F_{hs}, with the theoretical diagonal and horizontal forces F_{ns} and F_{hs} throughout the struts that satisfied the STM provisions in the ACI-318-14 (A-2). The forces consentrated in the nodal zone 1 and 2 are illustrated in Figure 23, 24 and 25.

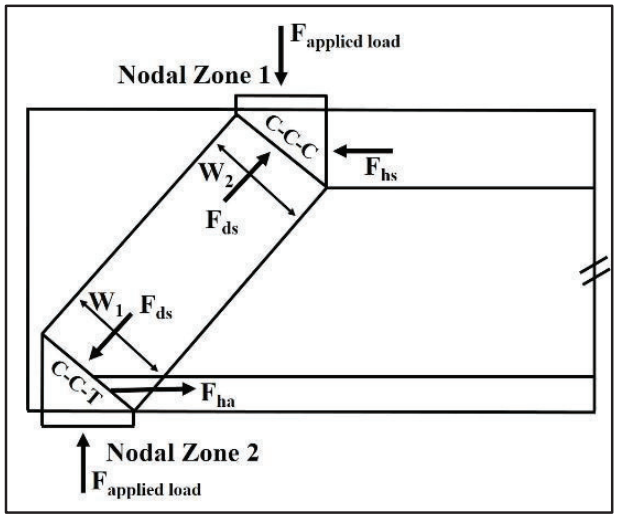

Figure 23: STM model's forces in nodal zone1 and 2

- The theoretical diagonal strut force (F_{ns}), recalling equations (2) and (3) in chapter 3:

$$F_{ns} = f_{ce}\, A_{cs}$$

Where:

$$F_{ce} = 0.85\, \beta_s f'_c$$

According to ACI-318-14 provisions and since the diagonal struts in the beams are crossed by inclined cracks, the value of β_s is given as 0.6. The used concrete compressive strength is 50.98 MPa. In equation, from geometry, the angle of the diagonal strut α is equal to 38.04°. The area of the diagonal strut (A_{cs}) is the result of multiplying the least width of the strut W_{s1}, W_{s2} by the depth of the strut, which equals to 150 mm.

$$tan\, \theta_s = [\, d - h_n/2]/a \qquad (11)$$

$$W_{s1} = l_b \sin(\alpha) + h_a \cos(\alpha) \quad (12)$$

$$W_{s2} = l_b \sin(\alpha) + h_s \cos(\alpha) \quad (13)$$

Substituting the givens in 11, 12 and 13 equations

$$tan\,\theta_s = \frac{\left[215 - \frac{52}{2}\right]}{241.5} = 0.782$$

$$\theta_s = 38.04\,°$$

$$W_{s1} = 40\sin(38.04) + 90\cos(38.04) = 95.52\ mm$$

$$W_{s2} = 60\sin(38.04) + 52\cos(38.04) = 77.92\ mm$$

$$\therefore F_{ce} = 0.85 * 0.6 * 50.98 = 25.99\ \text{MPa}$$

$$\therefore F_{ns} = 0.75 * 25.99 * \frac{77.92*150}{1000} = 227.82\ \text{kN}$$

Now, using FBD of nodal zone1 that shown in Figure 24, the resulted actual forces F_{ds} and F_{hs} that applied on diagonal and horizontal struts are obtained as following

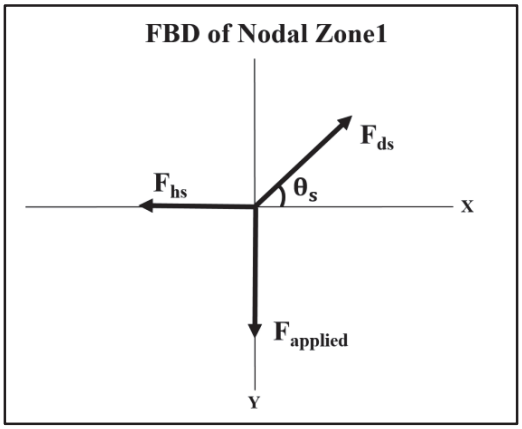

Figure 24: FBD of nodal zone 1

$$\sum Fy = 0$$

$$F_{ds}\sin(\theta_s) - F_{applied} = 0$$

$$\therefore F_{ds} = \frac{F_{applied}}{\sin(\theta_s)} \quad (14)$$

$$\sum Fx = 0$$

$$F_{ds}\cos(\theta_s) - F_{hs} = 0$$

$$\therefore F_{hs} = \frac{F_{applied}}{\sin(\theta_s)} * \cos(\theta_s) \qquad (15)$$

- Checking for actual diagonal strut force (F_{ds}) which was calculated using equation 14 as:

$$\therefore F_{ds} = \frac{118}{\sin 38.04} = 191.5\ KN$$

$$\therefore F_{ns} > F_{ds}$$

$$\therefore 227.82 > 191.5 \text{ kN O. K}$$

- The theoretical horizontal strut force (F_{hs}), recalling equations (2) and (3) in chapter 3:

$$F_{hs} = f_{ce}\, A_{cs}$$

Where:

$$F_{ce} = 0.85\, \beta_s f'_c$$

β_s is equal to 0.6, and the used compressive strength of strut is 50.98 MPa. From geometry, the angle of the diagonal strut α is equal to 38.04°. The area of the horizontal strut (A_{cs}) is the result of multiplying the the height of horizontal strut (h_s) by the width of the strut 150 mm.

$$\therefore F_{ce} = 0.85 * 0.6 * 50.98 = 25.99 \text{ MPa}$$

$$\therefore F_{ns} = 0.75 * 25.99 * \frac{52*150}{1000} = 152 \text{ kN}$$

- Checking for actual horizontal strut force (F_{hs}) which was calculated using equation 15 as:

$$\therefore F_{hs} = \frac{F_{applied}}{\sin(\theta_s)} * \cos(\theta_s)$$

$$\therefore F_{hs} = \frac{118}{\sin(38.04)} * \cos(38.04) = 150.8$$

$$\therefore F_{ns} > F_{hs}$$

$$\therefore 152 > 150.8 \text{ kN O. K}$$

B- Checking the Strengths of Tie

This step is pointing out the ability of tie element in the STM truss to resist the actual applied force generated. This step is fulfilled by obtaining the actual force that pointed on tie by the applied load and compare it to the theoretical nominal strength of the tie using ACI-318-14's equation to ensure an adequate resisting force in the tension element of the truss.

The theoretical nominal strength of the tie is given as a result of the summation of yield strength of the conventional reinforcement used in the beams and the prestressing reinforcement force by recalling equation (6) in chapter 3:

$$F_{nt} = A_{ts} f_y + A_{tp}(f_{se} + \Delta f_p)$$

A_{ts} is the area of the BFRP reinforcement bars used in the beam. The yield strength of the bars (f_y) is equal to 1282 MPa. Since there no prestresing reinforcement used in all beams, the value of the A_{tp} is equal to zero.

- The theoretical nominal strength of the tie F_{nt} is calculated using equation (6) as following

$$\therefore F_{nt} = \frac{0.75 * 1282 * 157}{1000} = 151\ KN$$

Now, using FBD of nodal zone 2 that shown in Figure 25, the resulted actual force F_{ha} that applied on horizontal tie is obtained as following

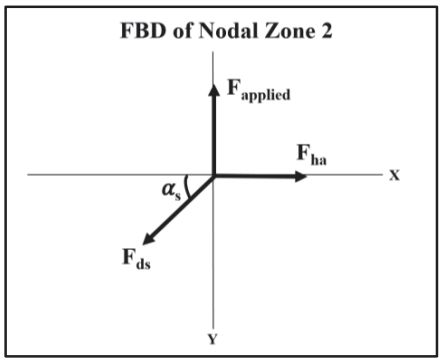

Figure 25: FBD of nodal zone 2

- Checking for horizontal tie force (F_{ha})

$$\therefore F_{ha} = \frac{118}{\sin(38.04)} * \cos(38.04) = 150.81$$

$$\therefore F_{ns} > F_{hs}$$

$$\therefore 151 > 150.81 \text{ kN O. K}$$

C- Checking the strength of nodal zones.

The actual dimension of the outer bearing plates used in the test was measured to be 60 mm. In this step, a checking of the theoretical outer dimensions is executed as well as a checking for the capacity of inner plates that exposed to horizontal and diagonal struts forces is performed based on the proposed STM provisions that implemented to nodal zones 1 and 2, which have (C-C-C) and (C-C-T) forces classification, respectively. Figure 26 illustrates the inner and outer plates of nodal zone 1 and 2.

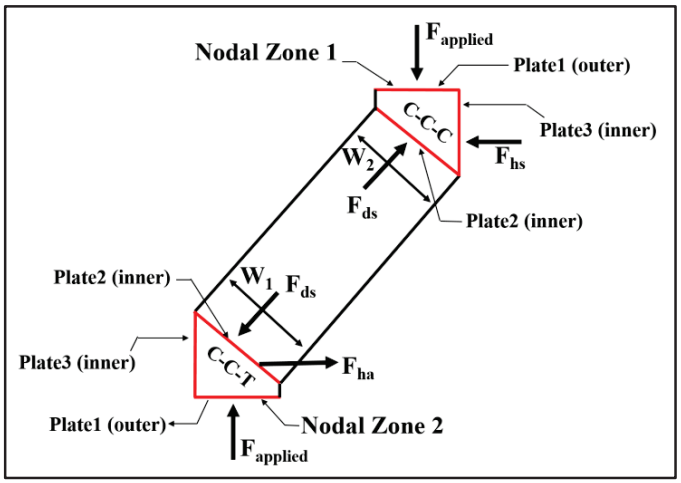

Figure 26: Inner and outer plates of nodal zones 1 and 2

- Strength of outer bearing plates in nodal zone1 and 2, recalling equations (7) and (8) in chapter 3:

$$F_{nn} = f_{ce} A_{nz}$$

Where:

$$F_{ce} = 0.85\,\beta_n\,\mathrm{f'c}$$

According to forces classification, ACI-318-14 suggested the value of $\beta_n = 1$ for outer bearing plate 1 and $\beta_n = 0.85$ for outer bearing plate 2, which used to estimate the effect of the anchorage of ties on the effective compressive strength of the nodal zone. Moreover, the used f'_C is 50.98 MPa.

After substituting all givens in equation (7) and (8) and solving the equation, the theoretical dimensions for outer bearing plates 1 and 2 is found to be:

$$118 * 1000 = 0.85 * 1 * 50.98 * 150 * 0.75 * l_{bmin}1$$

$$118 * 1000 = 0.85 * 0.8 * 50.98 * 150 * 0.75 * l_{bmin}2$$

$$lb_{min}1 = 24.2\,mm < 60\,mm\;\; O.K$$

$$lb_{min}2 = 30.3\,mm < 40\,mm\; O.K$$

- Strength of inner bearing plates of nodal zone 1 and 2

According to Figure 26, the demand on inner plate 1 is produced by diagonal strut force F_{ds} on the diagonal strut area and found to be

$$\sigma_{demand\ of\ P2} = \frac{F_{ds}}{Area\ of\ diagonal\ strut\ (a_1)} \qquad (16)$$

$$\therefore \sigma_{demand\ of\ P2} = \frac{191.5*1000}{77.92*150} = 16.38\,MPa$$

According to STM provision in ACI318-14 the compressive force capacity of inner plate1 is given by equation (8) in chapter 3 as:

$$F_{ce} = 0.85\,\beta_n\,\mathrm{f'c}$$

$$\therefore F_{ce} = 0.85 * 1 * 50.98 = 43.33MPa$$

$$\therefore \sigma_{demand\ of\ P1} < \sigma_{capacity\ of\ P1}\ \text{O.K}$$

The same procedure is followed in checking the strength of inner plates 2 and 3. Table 12 summarize the demand forces and the corresponding capacities in nodal zones 1 and 2. It was ensured that a reserved strength is guaranteed in all bearing plates in nodal zones 1 and 2.

Table 12: Summary of forces demand and plates capacities in nodal zone 1 and 2

Nodal Zone	Bearing plate	Strength (MPa)		Status
Nodal Zone1	Plate 1 (outer)	theoretical	24.2	O.K
		actual	60	
	Plate 2 (inner)	demand	16.4	O.K
		capacity	43.3	
	Plate 3 (inner)	demand	19.3	O.K
		capacity	43.3	
Nodal Zone2	Plate 1 (outer)	theoretical	30.3	O.K
		actual	40	
	Plate 2 (inner)	demand	13.4	O.K
		capacity	34.7	
	Plate 3 (inner)	demand	11.2	O.K
		capacity	34.7	

Chapter 5. Discussion of Results

5.1. Load VS midspan Deflection Behavior

5.1.1. Effect of basalt microfibers. The load-deflection graph of Group 1 beams shown in Figure 19 (a) illustrate the load response of beams with basalt and synthetic microfibers in comparing to plain concrete beam. The addition of basalt and synthetic microfibers mainly boost the stiffness of BFRP beams at all load stages. The overall stiffness of beam BN2T10_1.15 that contains basalt microfiber was similar to the beam SN2T10_1.15 that contains synthetic microfiber. However, BN2T10_1.15 and SN2T10_1.15 showed a higher stiffness and less mid-span deflection than PN2T10_1.15 plain beam. For instance, at 150 kN service load, addition of basalt microfibers increased the overall stiffness and thus decreased the mid-span deflection of BN2T10_1.15 beam by 31.2% in comparison with PN2T10_1.15 plain beam. On the other hand, the addition of synthetic microfibers in beam SN2T10_1.15 improved the overall stiffness by 28.6% compared to the plain concrete beam PN2T10_1.15. The improvement in stiffness for FRC beams is attributed to the effective bridging mechanisms that transfers the internal stresses from tips of the fibers to the surrounding concrete by the surface friction of basalt and synthetic microfibers.

5.1.2. Effect of shear span-to-depth ratio (a/d). The overall stiffness of Group 2 beams is influenced by varying the shear span-to-depth ratios. Increasing a/d ratio from 1.15 to 1.48 and 1.82 has a direct correlation in decreasing the stiffness of beams due to the development and widening of diagonal cracks that cause a higher mid-span deflection as shown in Figure 19 (b). At any given load, the measured deflection was decreased as the shear span-to-depth ratio decreased. For instance, using the same reinforcement ratio of (R2 = 0.7), at 150 kN the deflection of beam BN2T12_1.82 which found to be 11.03 mm has decreased by 37.5% to reach 6.89 mm in BN2T12_1.48 beam and by 50.8% to reach 5.42 mm in BN2T12_1.15 beam. This decrease in the beams' deflection (i.e., increase in stiffness) was developed due to the increase in the angle between diagonal strut and horizontal tie as the shear span-to-depth ratio decreases from 1.82 to 1.48 and 1.15. Hence, more effectual arch action was produced in the shear span areas. Which led to more load carrying capacity and less mid-span deflection in the beams.

The load-deflection results of Group 2 beams were compared to a previous study conducted by Abed et al.[68]. The study contains three similar short BFRP reinforced beams but cast with plain concrete. The load verses midspan deflection curves for group 2 beams and Abed's plain concrete beams are plotted as shown in figure 27. The comparison showed that with the same a/d ratios of 1.15, 1.48 and 1.82 the presence of fibers in Group2 beams allows to reach a higher mid-span deflection and overall stiffness than plain concrete beams by 9.7 %, 34.2 % and 55.5% respectively.

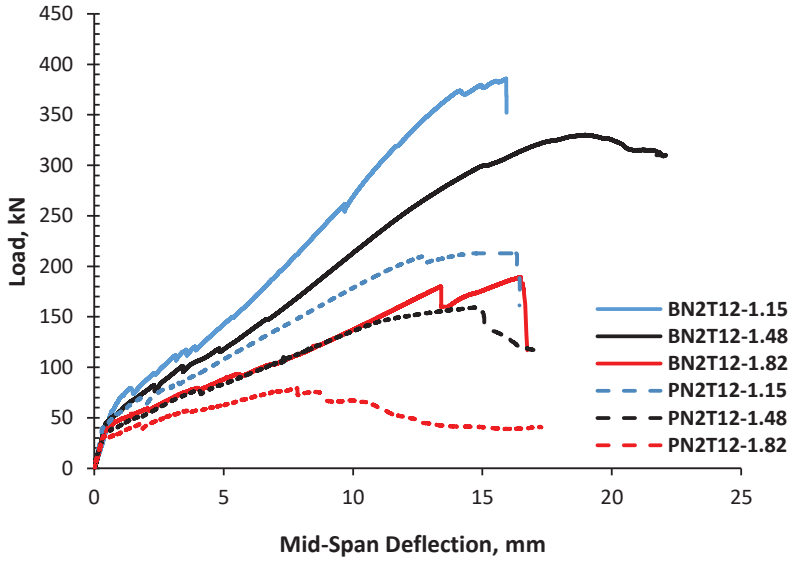

Figure 27: Load vs Mid-span deflection for group 2 beams with and without fibers

5.1.3. Effect of reinforcement ratio (ρ). The effect of reinforcement ratio on mid-span deflection of the tested beams is examined in Group 3 beams. Generally, the results showed that the reinforcement ratio directly affects the post cracking behavior in short beams. A similar deflection was observed for all beams until the formation of initial crack, after which the cracks started being wider at a smaller reinforcement ratio. However, the results showed that beams reinforced with higher reinforcement ratio are more capable to retain their stiffness during load increments and eventuate exhibiting less deflection, while beams with less reinforcement ratio are suffered from the reduction in their stiffness as shown in Figure 19(c). For example, at a service load of

200 kN (0.6 of the ultimate load), the measured mid-span deflection of BN2T10_1.15 was 8.73 mm while the corresponding mid-span deflections of BN2T12_1.15 and BN2T16_1.15 were found to be 7.38 and 5.79 mm, respectively.

The load-deflection responses of beams BN2T10_1.15 and BN2T12_1.15 were compared to Abed et al.[68] study's beams that have similar beam configurations excluded of basalt microfibers. The maximum midspan deflection of both sets were relatively close with a constant reinforcement ratios of 0.49 and 0.70.

5.1.4. Effect of concrete compressive strength (f'_C). According to Figure 19 (d), it can be observed that both beams of BH2T10_1.15, which made of high compressive strength concrete and beam BN2T10_1.15 that made using normal concrete strength have similar linear load-deformation trend during service and ultimate loads. Results that are more significant were noted by utilizing high strength concrete in enhancing the shear capacity of the beams by increasing the load carrying capability and improving the failure mechanism of high strength beam BH2T10_1.15.

5.2. Failure Mode

In the early stage of the loading, all beams have witnessed a formation of vertical cracks initiated at the bottom of the beams and concentrated in the pure bending region. With a further increase in the load, diagonal cracks were formed in the shear span between the two loading points and supports. Those inclined cracks started in the mid-high near the points loads, propagated towards the supports with the increasing load until they stabilize, and stopped propagating while widening until failure. All beams have exhibited a reserved strength after the final widening of diagonal strength due to the effective arch action. The same failure modes was reported by other researchers[1],[46],[47].

It was observed that Group 1 beams that reinforced with basalt and synthetic microfibers have failed in more ductile manner than plain concrete beam. After initial cracks in flexural region, beams reinforced with microfibers have continued to resist increasingly more load while sustain considerable deformation, describing the overall member ductility that can be attain from adding those microfibers to the concrete. BN2T10_1.15 that reinforced with basalt microfibers failed with a higher overall load than SN2T10_1.15. However, the presence of both basalt fibers in BN2T10_1.15 and

synthetic fibers in SN2T10_1.15 beam have helped in delaying cracks after the complete formation of diagonal cracks by the role of bridging mechanism, resulting in less deflection and more load carrying capacity than PN2T_1.15. Nevertheless, BN2T10_1.15 beam failed at maximum applied load of 330.82 kN corresponding to a maximum deflection of 15 mm while synthetic beam failed by having a less load carrying capacity at maximum applied load of 309.79 kN corresponding to a maximum deflection of 15.55 mm. As shown in Figure 28, Group 1 beams have failed similarly by a brittle crashing in the beam support area at maximum load accomplished by splitting of diagonal compression strut.

(a)

(b)

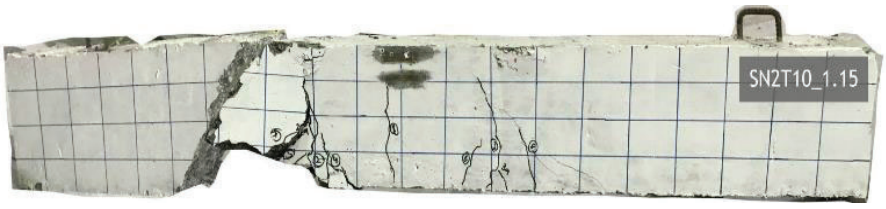

(c)

Figure 28: Beams failure mode (group1), (a) BN2T10_1.15, (b) PN2T10_1.15, (c) SN2T10_1.15

Group 2 beams that have different shear span-to-depth ratios of 1.15, 1.48 and 1.82 have failed in similar manner by developing major diagonal cracks that extending mainly from one of the points load directly to the support as shown in Figure 28. This major crack start widening during the load increasing until causing splitting of BFRP bars and concrete in the diagonal strut. BN2T12_1.15 and BN2T12_1.48 beams that have shear span of 246 mm and 317 mm, respectively, failed initially by developing of

diagonal crack through the compression strut followed by concrete crushing in the same struts. However, in comparing to BN2T12_1.15 the increase in BN2T12_1.48's shear span lead to decrease the angel between diagonal compression strut and horizontal tie from 36.29° to 29.77°. The lower angel in BN2T12_1.48 result in a lower capability of resisting the increased load due to the reduce in overall arch action mechanism. However, the presence of basalt microfibers provides BN2T12_1.48 and BN 2T12_1.82 beams an additional ductility to sustain load increments before failure, after which the major diagonal crack formed. BN2T12_1.82 beam that has the highest shear span-to depth ratio exhibited a shear failure by developing a diagonal shear cracks prior to concrete crushing in the top horizontal strut. Shear span-to-depth ratio that close to two in BN2T12_1.82 results in excessive reduction in load carrying capacity since that a/d ratio is closer to 2.5 which makes the beam behave more as a slender beam rather than deep beam as shown in Figure 29. Similar behavior reported by other researchers [48][46].

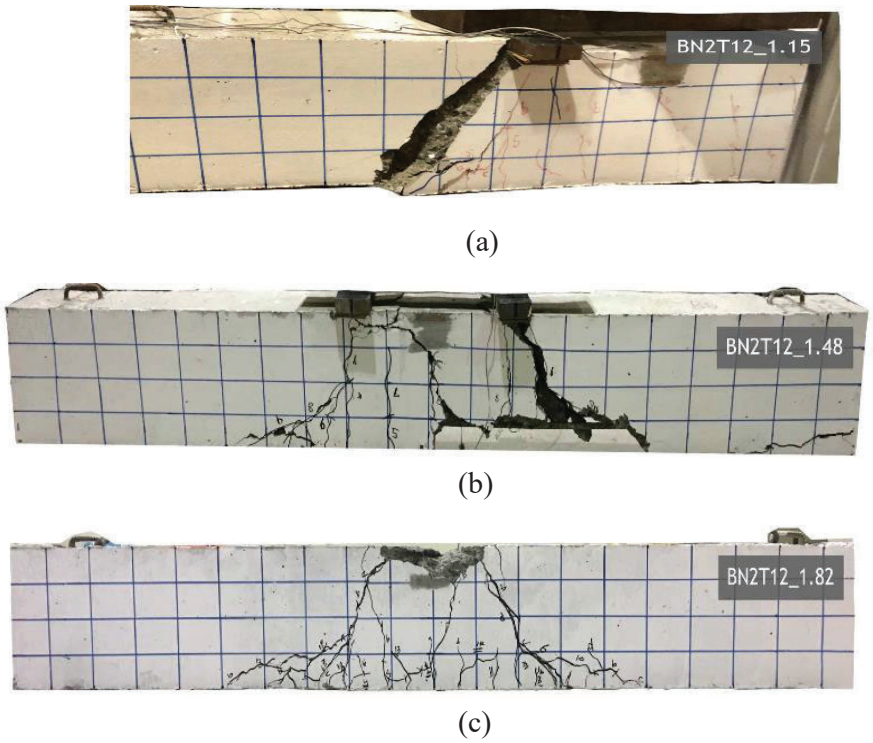

Figure 29: Beams failure mode (group 2), (a) BN2T12_1.15, (b) BN2T12_1.48, (c) BN2T12_1.82

On the other hand, Group 3 beams that have different reinforcement ratios of 0.49, 0.70 and 1.26 exhibited a typical shear failure regardless of the variation in reinforcement ratios. All beams failed by developing a wide diagonal crack extending from loading points to the beam support causing diagonal split in only one side of the beams as shown in Figure 30.

(a)

(b)

(c)

Figure 30: Beams failure mode (group 3), (a) BN2T10_1.15, (b) BN2T12_1.15, (c) BN2T16_1.15

The same shear failure modes observed in Group 4 beams that demonstrated in Figure 31. BN2T10_1.15 and BH2T10_1.15 that contains normal concrete and high strength concrete, respectively, exhibited developing a diagonal shear crack propagating until failure. It was noticed that the angel of shear failure in BH2T10_1.15 decreased as the compressive strength increased. This is attributed to the increase in the shear capacity after using higher compressive strength concrete that work more efficiently with basalt microfibers.

(a)

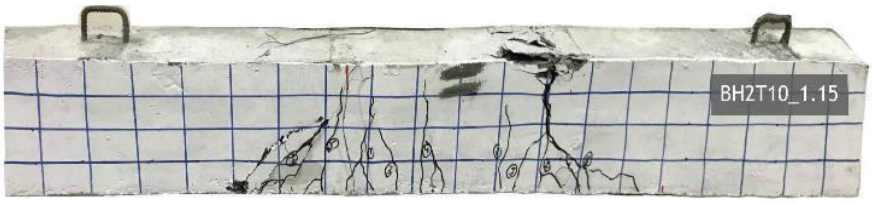

(b)

Figure 31: Beams failure mode (group 4), (a) BN2T10_1.15,
(b) BH2T10_1.15

5.3. Strain Response of BFRP Bars

The load versus strain plots of all BFRP bars utilized in tested beams exhibited similar characteristics. For all eight beams, at initial load stage, the reinforcement strain varied linearly up to the formation of the first diagonal shear crack. After that, the strains in BFRP bars become aligned with uniform increase, which proves the formation of the tie action. Then the test variables played a role in characterizing the final strain behavior of BFRP bars with increased load until failure occurred. Figure 21 demonstrated the relationship between applied load and strains in BFRP bars.

The addition of basalt and synthetic microfibers affected the strain responses in BFRP bars. In Group 1 beams, at maximum load, the addition of basalt microfibers in beam BN2T10_1.15 increased the mid-span strain of BFRP bars by 16.8% and 27.9% with comparison to beam SN2T10_1.15 that contains synthetic microfibers and plain beam PN2T10_1.15, respectively. The effect of synthetic microfibers in increasing the strain response in BFRP bars is lower than its counterpart that contains basalt microfibers. This inability of increase in BFRP strain by the addition of synthetic microfibers explained by the good impact stiffness of synthetic microfibers at initial load stage only in comparing with basalt microfibers with a low modulus of elasticity. The same observation was reported by Zhang et al.[69]. In Group 2 beams, it was

observed that the increase in shear span-to-depth ratio from 1.15 for beam BN2T12_1.15 to 1.48 and 1.82 for beams BN2T12_1.48 and BN2T12_1.82 increases the BFRP strain by 21.30 and 29.51%, respectively.

A significant influence of reinforcement ratio on the bars strain is also recorded. In Group 3 beams, at any loading stage, the BFRP bars strain is decreased as the reinforcement ratio increased. This increase in BFRP bars strain is continued over all loading stages until failure takes place. For instance, at 200 kN increasing the reinforcement ratio by 30% from 0.49 for beam BN2T10_1.15 to 0.70 for beam BN2T12_1.15 lead to strain reduction in BFRP bars by 23.6 %. Additional increase of the ρ ratio by 44.4% to reach 1.26 in beam BN2T16_1.15 resulted in 39.8 % reduction in BFRP bars strain. Similar strain responses were reported by other researchers [1], [47].

In Group 4 beams, a reduction in BFRP bars strain is observed by the using of high concrete compressive strength. At service load of 200 kN BH2T10_1.15 exhibited an 18% reduction in BFRP bars strain in comparing with beam BN2T10_1.15.

5.4. Strain Response of Concrete

All tested beams showed similar concrete strain responses in the pre-cracking stage. At the post-cracking stage, the concrete compression strain increased until the complete shear failure occurred. The applied load and strain's relationship of all tested beams is plotted in Figure 21.

The maximum recorded concrete compression strains in all tested beams were significantly below the concrete crushing strain. The measured concrete strain in the maximum bending moment section was approximately less than 1800 micro-strain, which is less than the maximum failure strain of concrete, indicating that the modes of failures were shear rather than flexure.

Group 1 beams that contain basalt and synthetic microfibers experienced higher strain in concrete compared to its plain counterpart beam. For instance, at the maximum load, adding basalt microfibers in beam BN2T10_1.15 increased concrete strain by 67.6% with comparison to beam SN2T10_1.15. The increase in concrete strain in BN2T10_1.15 beam attributed mainly to the fact that basalt microfibers have higher

tensile strength and modulus of elasticity than synthetic microfibers, which help in controlling cracks propagating as well as distribute stresses more efficiently into concrete particles, and thus, maintain more load. The same effect of microfibers is reported by Altoubat et al.[24].

The main variable affected the load-strain responses in concrete strain of the tested beams is the variation in reinforcement ratio. In Group 3 beams, at any load in the post-cracking stage, the strain in concrete is decreased as the reinforcement ratio increased. For example, at 200 kN service load, concrete strain in beams BN2T12_1.15 and BN2T16_1.15 decreased by 6.5% and 19.5%, ,respectively, after increasing the reinforcement ratio in beam BN2T10_1.15 from 0.49 to 0.70 and 1.26. The same observation was reported by Elsayed et al.[1].

5.5. Effect of Test Variable on Shear Capacity

5.5.1 Effect of basalt microfibers. Group 1 beams capture the effect of using basalt and synthetic microfibers on the shear behavior of the tested beams. The effect of using basalt microfibers on shear behavior is captured by comparing its ultimate shear strength to that of synthetic microfibers and plain specimens. The results showed a significance difference in load carrying capacity in the two beams that containing basalt and synthetic microfibers compared to the plain beam. The variation of experimental ultimate shear strengths in beams of Group 1 is represented in Figure 32.

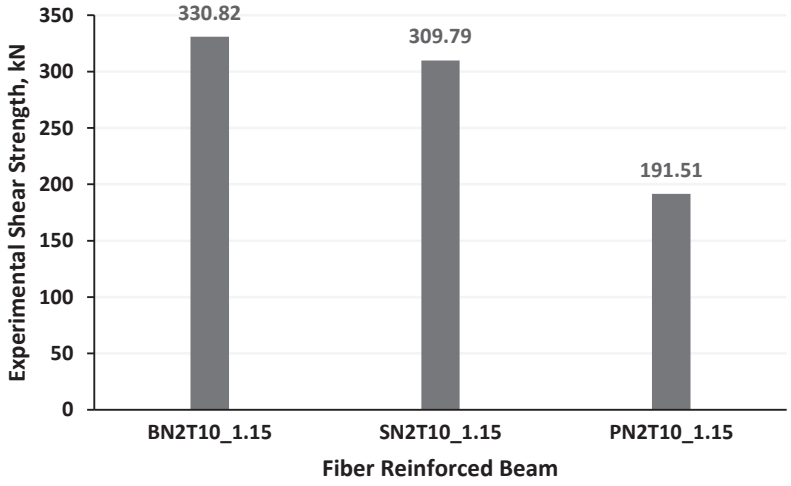

Figure 32: Experimental Shear Strength of Group 1 Beams

According to Figure 32, beam BN2T10_1.15, which contains basalt microfibers, exhibited a higher load carrying capacity than SN2T10_1.15 beam, which contains synthetic fibers, and plain concrete beam PN2T10_1.15 by 6.4% and 42.1%, respectively. In comparison with plain concrete, the higher contribution to the load capacity that offered by beams BN2T10_1.15 and SN2T10_1.15 is due to the presence of basalt and synthetic microfibers which mainly bridging the micro-cracks by efficiently transferring the stress to the surrounding concrete.

BN2T10_1.15 beam has a relatively higher load resisting than SN2T10_1.15 beams. This effect is attributed to the higher tensile strength of basalt microfibers that has superior potentials in arresting the stress concentration on the cracks tips and convert it to the concrete, hence restrain the propagation of more cracks, and delayed the failure of beams more effectively. However, BN2T10_1.15 and SN2T10_1.15 eventually failed as the load exceeding a certain value that cannot be resisted by fibers, leading to a brittle failure. The same phenomenon of basalt and synthetic microfibers behaviors was reported by Zhang et al [69].

Furthermore, the effect of basalt microfibers in enhancing the load carrying capacity was captured by comparing the ultimate loads of Group 2 beams with similar group of three BFRP beams that cast with plain concrete (NRC) in a study conducted by Abed et al.[68]. The result revealed that the presence of basalt microfibers significantly improves the load carrying capacity of beams: BN2T12_1.15, BN2T12_1.48 and BN2T12_1.84 by 44.8 % (from 213 kN to 385.79 kN), 51.8% (from 159.2 kN to 330.15 kN) and 58.0% (from 79.5 kN to 189.39 kN), respectively.

5.5.2 Effect of shear span-to-depth ratio (a/d). The different shear span-to-depth ratio (a/d) exhibited an influential effect on the ultimate shear capacity of the tested beams. In Group 2 beams, with a constant reinforcement ration and fiber type, an overall improvement in load carrying capacity was observed as the shear span-to-depth ratio decreased. The effect of decreasing the span-to-depth ratio (a/d) on increasing the load carrying capacity of all tested beams is illustrated in Figure 33.

In Group 2 beams, decreasing a/d ratio in beam BN2T12_1.82 by 18.7% from 1.82 to 1.48 in beam BN2T12_1.48, increased the ultimate shear capacity by 40% from 189.39 kN to 330.15 kN. Further decrease in a/d ration by 22.3% to reach 1.15 in beam

BN2T12_1.15 resulted in raising the maximum load resisting capability from 330.15 kN to 385.79 kN (14.4% increase).

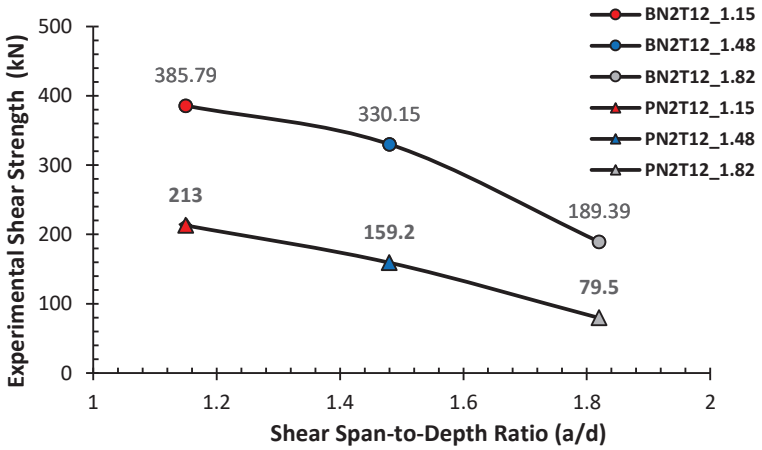

Figure 33: Effect of a/d on the shear capacity of BFRC deep beams.

It is suspected that increase in the ultimate load is a direct result of decreasing the distance between the supports and the applied loads, which lead to increase the angle between diagonal compression strut and the tension tie resulted in enhancing the arch mechanism in the beam. Arch mechanism is responsible of transmitting the applied load directly to the supports through the diagonal compression struts. In addition, the general stiffness of the three beams is decreased as the shear span-to-depth ratio (a/d) increased. The same shear span-to-depth effect on shear behavior of deep beams were reported by other researchers [1], [46], [48].

5.5.3. Effect of reinforcement ratio (ρ). Test results showed that the ultimate shear capacities of Group 3 beams is increased with the increase of the reinforcement ratio ρ, for the same shear span-to-depth ratio and fiber type used. Increasing ρ by 30% from 0.49% in beam BN2T10_1.15 to 0.70% in beam BN2T12_1.15 resulted in 14.2% improvement in load carrying capacity (330.82 verses 385.79 kN respectively).

Additional increase in ρ by 44.4% from 0.70 in beam BN2T12_1.15 to 1.26 in beam BN2T16_1.15 did not produce any further enhancement. This modest change in the percentage of the accomplished ultimate shear capacities by changing ρ agreed with the Ashour's [70] finding, which noted that increasing the longitudinal reinforcement

in deep beams increases the ultimate shear capacity up to a certain limit after which no improvement in shear strength can be attained.

However, the increase in the ultimate shear capacity by increasing ρ is attributed mainly to the increase in the depth of the compression segment in the tested beams at failure when the beam section intending to balance the location of neutral axis with the increased tension forces in horizontal tie. The same observation was reported by other researchers [46]. Figure 34 illustrated the effect of reinforcement ratio ρ on the ultimate shear strength of tested beams. The upper beams in Figure 34 were cast using basalt fiber reinforced concrete mix (BFRC) while the lower beams were cast using concrete mix with normal compressive strength (NRC).

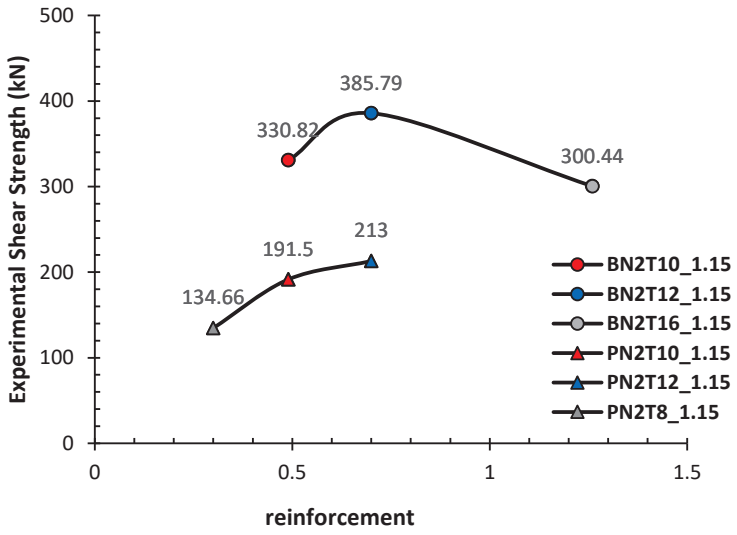

Figure 34: Effect of ρ on the shear capacity of BFRC deep beams

5.5.4. Effect of concrete compressive strength (f'_C). Changing in the concrete compressive strength f'_C of the tested beams is observed to have a significant impact in improving the ultimate shear capacity of the BFRP-reinforced deep beams. With constant shear span-to-depth ratio (a/d) and reinforcement ratio ρ, increasing the f'_C by 11.87% from 50.67 MPa in beam BN2T10_1.15 to 57.5 MPa in beam BH2T10_1.15 resulted in 20.26% increase in the ultimate shear strength.

5.6. Shear Capacity using Strut and Tie Model

The strut-and-tie model in ACI 440.1R-15 guide for structural elements reinforced with FRP is not yet considered. Therefore, strut-and-tie model in ACI-318-14 is adopted in the study. The predicted ultimate shear strength of tested beams presented by STM in ACI-318-14 is evaluated and summarized in Table 13

The prediction of ultimate shear strength was based on the most critical region of strut, tie and nodal zone, that reaches its load limits earlier and governs the failure. However, the results in Table 13 showed that the load prediction according to strut and tie model in ACI-318-14 have conservative estimation of the ultimate shear loads of the most tested beams compared to the experimental results. The experimental results show that the tested beams yielded a greater load than ACI-318-14 loads with average ratio of 1.22.

Table 13: Ultimate shear capacity of STM model

Sr#	Beam	Failure Load P_{exp} (kN)	Failure Load P_{ACI} (kN)	P_{exp} /P_{ACI}
1	BN2T10_1.15	330.82	236	1.40
2	BN2T12_1.15	385.79	311	1.24
3	BN2T16_1.15	300.44	311	0.97
4	BN2T12_1.48	330.15	254	1.30
5	BN2T12_1.82	189.39	194	0.98
6	BH2T10_1.15	414.88	239	1.74
7	PN2T10_1.15	191.51	229	0.84
8	SN2T10_1.15	309.79	234	1.32

The limitation in predicting the ultimate shear capacity in STM model in ACI-318-14 explained by the fact that STM model depends mainly on the concrete compressive strength ACI 440.1R-15 and the beam's geometry in evaluating the struts strength without considering the presence of main longitudinal reinforcement or the addition of microfibers. This fact is proven in beam BN2T12_1.15 and BN2T16_1.15, increasing the reinforcement are by 43.8% resulted in similar ultimate shear capacity. On the other hand, STM model in ACI-318-14 accounts for absence of web

reinforcement through the strength reduction factor B_s. Hence, neglecting the high axial strength of BFRP bars and the presence of basalt microfibers in STM model resulted in lower ultimate shear strength in comparison to the experimental results.

The calculated loads of diagonal and horizontal struts and horizontal tie by STM model are summarized in Table 14. From elements load results, it was noticed that the diagonal strut loads are higher than the horizontal strut and tie loads and this explains the formation of arch action in deep beams that resulted in diagonal shear cracks that shown in the experimental work. This fact in STM model's elements loads agreed completely with the experimental failure modes. In addition, the diagonal struts reached only 80.2-93.4% of their ultimate loads. Increasing the applied load on diagonal struts resulted in simultaneous failure in horizontal strut and tie as a result of neglecting the FRP microfibers in STM model that was proven to delayed the cracks and improve the overall shear behavior of the beam by increasing ultimate shear load in experimental results.

The effect of changing the test variables on the ultimate shear strength provided by STM model in ACI-318-14 were similar to those outcomes on the experimental ultimate shear strength. For instance, in Group 1 beams, the addition of basalt and synthetic microfibers resulted in reasonable increasing in the ultimate shear strength of tested beams Although ACI-318-14 were conservative since that the experimental results have much higher reserved strength than ACI-318-14 predictions. The ultimate shear strengths of beams BN2T10_1.15 and SN2T10_1.15 were 236 and 234 kN respectively as compared to 229 kN in plain beam PN2T10_1.15. it was noticed that STM model did not accounts for the effect on adding basalt and synthetic microfibers to the concrete mix as depends mainly on the shear span-to-depth ratios (a/d) and concrete compressive strength (f'_c).

However, the estimated shear strengths by ACI of Group 2 and Group 3 that have different shear span-to-depth ratios (a/d) and different reinforcement ratios σ were in agreement with their effects on experimental ultimate shear strengths. In Group 4 beams, the effect of adding basalt and synthetic microfibers on improving the ultimate shear strength of high strength concrete beams was not captured by STM model in ACI-318-14.

Table 14: Predicted loads of strut-and-tie elements

	diagonal Strut Loads,(kN)			Horizontal Strut Loads, (kN)			Horizontal Tie Loads, (kN)		
Beam	**Applied**	**Limit**	**%**	**Load**	**Limit**	**%**	**Applied**	**Limit**	**%**
BN2T10_1.15	191.5	227.9	1.190	150.8	152	1.008	150.8	151	1.001
BN2T12_1.15	262.7	281.4	1.071	211.8	225	1.062	211.8	222	1.048
BN2T16_1.15	261.6	281.2	1.075	210.3	228	1.084	210.3	355	1.688
BN2T12_1.48	255.7	280.1	1.095	221.9	222	1.000	221.9	222	1.000
BN2T12_1.82	227	261.4	1.152	205.3	206	1.003	205.3	222	1.081
BH2T10_1.15	192.2	239.7	1.247	150.5	151	1.003	150.5	151	1.003
PN2T10_1.15	189.4	207.6	1.096	150.9	152	1.007	150.9	151	1.001
SN2T10_1.15	190.9	222.5	1.166	150.8	153	1.015	150.8	151	1.001

Chapter 6. Conclusion

In this research, an experimental investigation was conducted to study the effect of new basalt microfibers on the shear response of short beams reinforced longitudinally with BFRP bars. Eight short beams were cast and tested under four-point loading setup to assess different shear outcomes namely deflection responses, failure modes, strains in BFRP bars and concrete and ultimate shear capacities. Four groups of different test variables were considered in this study. Group 1 investigates the effect of adding basalt microfibers to the concrete mix as compared to synthetic microfibers and plain concrete. The effect of adding basalt microfibers to the concrete mix was further studied for BFRP reinforced deep beams by considering three different shear span-to-depth ratios (Group 2), three different reinforcement ratios (Group 3) and two different concrete compressive strengths (Group 4).

Moreover, an analytical prediction of shear responses using the Strut-and-Tie Modeling (STM) was carried out in accordance to ACI-318-14 provisions to evaluate the shear responses of tested beams and assess the capability of the STM method in validating the experimental results for the ultimate shear strength. Based on the theoretical and experimental results that presented in pervious sections, the following observations and conclusions can be drawn:

1. All tested beams exhibited bilinear responses until failure occurred. The tested beams showed similar behavior and stiffness up to the initiation of first crack, followed by gradual reduction in beams' stiffness and increasing in shear cracks propagation with different tendency based on their distinctive test variables.

2. The prevailing failure mode of all tested beams was shear failure characterized by propagation of a major diagonal shear crack followed by splitting between BFRP bars and concrete only, while some beams experienced similar shear failure shown as splitting between BFRP bars and concrete in addition to concrete crushing at diagonal strut. Only one beam failed by splitting and concrete crushing at the top fibers at ultimate.

3. The addition of basalt microfibers improved the overall stiffness by decreasing the mid-span deflection of the beams. The mid-span deflection and crack width of tested beams is decreased as the shear span-to-depth ration (a/d) decreased and reinforcement ratio increased ρ. Moreover, the high compressive strength of concrete had no effect on the stiffness and only increased ultimate load capacity of the beams.

4. Beam containing basalt microfibers exhibited higher mid-span strains in BFRP bars at maximum load in comparison to the synthetic and plain concrete beams by 16.8% and 27.9% due to the high tensile strength and modulus of elasticity of basalt microfibers. The BFRP strains were decreased as the reinforcement ratios ρ increased and shear span-to-depth ratios a/d decreased.

5. The addition of basalt microfibers has increased the concrete strain in general more than synthetic microfibers. This is due to the higher tensile strength of basalt microfibers that enhance cracks propagation control as well as distribute stresses more efficiently than synthetic microfibers.

6. The ultimate shear strength of tested beams was significantly increased by the addition of basalt microfibers with 42.1% more load carrying capacity than plain concrete beam. This enhancement attributed to the high ability of basalt microfibers in bridging the micro cracks by the efficient transferring of the stresses from tips of those cracks to the surrounding concrete. Hence, the propagation of more cracks will be restrained and overall load failure will be delayed.

7. The different shear span-to-depth ratios have significance impacts on the ultimate shear strength of BFRP reinforced deep beams. As the shear span-to-depth ratios decreased, the obtained ultimate shear strength increased significantly. This is attributed to the increased angle between diagonal compression strut and horizontal tie resulting in enhancing the arch mechanism and allow the beam to sustain more load capacity.

8. With constant shear span-to-depth ratios of 1.15,1.48 and 1.82 the addition of basalt microfibers has significance impact on increasing the mid-span deflection and overall beam stiffness by 9.7%, 34.2% and 55.5%, respectively with comparison to plain beams.

9. A higher ultimate shear strength of all tested beams is obtained by increasing the BFRP reinforcement ratio ρ until a certain limit only, after which no improvement in overall strength would be attained by any reinforcement ratio increments.

10. The predicted ultimate shear strength of BFRP reinforced short beams that contain basalt microfibers using STM model was conservative. This is due to the dependency of STM model on the concrete compressive strengths and the beam's geometry in evaluating the struts strengths without considering the presence of main longitudinal reinforcement or the addition of microfibers.

References

[1] A. K. El-sayed, E. F. El-salakawy, and B. Benmokrane, "Shear strength of fibre-reinforced polymer reinforced concrete deep beams without web reinforcement," *Canadian Journal of Civil Engineering*, vol. 39, no. 5, pp. 546–555, 2012.

[2] C. Shield, W. Gold, and T. Alkhrdaji, *Guide for the Design and Construction of Structural Concrete Reinforced with FRP Bars*, 1st ed. American Concrete Institute, 2015.

[3] H. Al-Ghanem, A. Al-Asi, M. Abdel-Jaber, and M. Alqam, "Shear and Flexural Behavior of Reinforced Concrete Deep Beams Strengthened with CFRP Composites," *Modern Applied Science*, vol. 11, no. 10, p. 110, 2017.

[4] J. P. Broomfield, *Corrosion of Steel in Concrete: Understanding, Investigation and Repair*, 2nd ed. CRC Press, 2006.

[5] A. Sagher and F. Abed, "Finite element parametric study of the shear behavior of GFRP-RC short beams," in *7th International Conference on Modeling, Simulation, and Applied Optimization (ICMSAO)*, 2017, pp. 1–5.

[6] G. Koch, M. Brongers, N. Thompson, and V. Yash, "Corrosion costs and preventive strategies in the United States," Virginia, United States, 2002.

[7] A. Rai and Y. P. Joshi, "Applications and Properties of Fibre Reinforced Concrete," *International Journal of Engineering Research and Applications*, vol. 4, no. 5, pp. 123–131, 2014.

[8] F. Yan, Z. Lin, and M. Yang, "Bond mechanism and bond strength of GFRP bars to concrete: A review," *Composites Part B: Engineering*, vol. 98, pp. 56–69, 2016.

[9] A. El Refai, F. Abed, and A. Altalmas, "Bond durability of basalt fiber-reinforced polymer bars embedded in concrete under direct pullout conditions," *Journal of Composites for Construction*, vol. 19, no. 5, pp. 1–11, 2015.

[10] A. Al-Tamimia, F. H. Abed, and A. Al-Rahmani, "Effects of harsh environmental exposures on the bond capacity between concrete and GFRP reinforcing bars," *Advances in Concrete Construction*, vol. 2, no. 1, pp. 1–11, 2014.

[11] F. H. Abed, A. Al-Rahmani, and A. H. Al-Rahmani, "Finite element simulations of the shear capacity of GFRP-reinforced concrete short beams," in *2013 5th International Conference on Modeling, Simulation and Applied Optimization (ICMSAO)*, 2013, pp. 1–5.

[12] R. Sonnenschein, K. Gajdosova, and I. Holly, "FRP Composites and their Using in the Construction of Bridges," *Procedia Engineering*, vol. 161, pp. 477–482, 2016.

[13] M. A. Masuelli, *Introduction of Fibre-Reinforced Polymers − Polymers and Composites: Concepts, Properties and Processes*, First. San Luis, Argentina: Intech Open, 2013.

[14] A. Al-Rahmani and F. H. Abed, "Numerical investigation of hybrid FRP reinforced beams," in *5th International Conference on Modeling, Simulation and Applied Optimization, ICMSAO*, 2013, pp. 1–6.

[15] F. Abed, M. Al-Mimar, and N. Tello, "Evaluation of BFRP RC beams under flexure," in *Advances in Science and Engineering Technology International Conferences (ASET)*, 2019, pp. 1–4.

[16] M. Peggy, "A hidden revolution: FRP rebar gains strength," *Composites world*, 2011. [Online]. Available: https://www.compositesworld.com/articles/a-hidden-revolution-frp-rebar-gains-strength. [Accessed: 08-Dec-2019].

[17] A. El Refai, F. Abed, and M. Asce, "Concrete Contribution to Shear Strength of Beams Reinforced with Basalt Fiber-Reinforced Bars," *ASCE Journal of Composites for Construction*, vol. 20, no. 4, pp. 1–13, 2016.

[18] F. Abed and A. R. Alhafiz, "Finite element simulation of the flexural behavior of BFRP-FRC beams," in *Advances in Science and Engineering Technology International Conferences (ASET)*, 2018, pp. 1–5.

[19] M. A. Issa *et al.*, "Shear Behavior of Basalt Fiber Reinforced Concrete Beams with and without Basalt FRP Stirrups," *ASCE Journal of Composites for Construction*, vol. 20, no. 4, pp. 1–11, 2016.

[20] D. Tomlinson and A. Fam, "Performance of concrete beams reinforced with basalt FRP for flexure and shear," *ASCE Journal of Composites for Construction*, vol. 19, no. 2, pp. 1–10, 2015.

[21] F. Elgabbas, E. A. Ahmed, and B. Benmokrane, "Flexural Behavior of Concrete Beams Reinforced with Ribbed Basalt-FRP Bars under Static Loads," *ASCE Journal of Composites for Construction*, vol. 21, no. 3, pp. 1–12, 2017.

[22] A. Razaqpur and B. Isgor, "Concrete contribution to the shear resistance of fiber reinforced polymer reinforced concrete members," *ASCE Journal of Composites for Construction*, vol. 8, no. 5, pp. 452–460, 2004.

[23] A. El Refai, F. Abed, and A. Al-Rahmani, "Structural performance and serviceability of concrete beams reinforced with hybrid (GFRP and steel) bars," *Construction and Building Materials*, vol. 96, pp. 518–529, 2015.

[24] S. Altoubat, A. Yazdanbakhsh, and K. A. Rieder, "Shear behavior of macro-synthetic fiber-reinforced concrete beams without stirrups," *ACI Materials Journal*, vol. 106, no. 4, pp. 381–389, 2009.

[25] F. Abed and A. R. Alhafiz, "Effect of basalt fibers on the flexural behavior of concrete beams reinforced with BFRP bars," *Composite Structures*, vol. 215, pp. 23–34, 2019.

[26] N. Elmessalami, A. El Refai, and F. Abed, "Fiber-reinforced polymers bars for compression reinforcement: A promising alternative to steel bars," *Construction and Building Materials*, vol. 209, pp. 725–737, 2019.

[27] A. Zaman, S. A. Gutub, and M. A. Wafa, "A review on FRP composites applications and durability concerns in the construction sector," *Journal of Reinforced Plastics and Composites*, vol. 32, no. 24, pp. 1966–1988, 2013.

[28] S. Raj, V. R. Kumar, B. H. B. Kumar, and N. R. Iyer, "Basalt: structural insight as a construction material," *Sadhana - Academy Proceedings in Engineering Sciences*, vol. 42, no. 1, pp. 75–84, 2017.

[29] H. C. Wu, *Advanced civil infrastructure materials Science , mechanics and applications*, 1st ed. Cambridge, England: Woodhead Publishing Limited, 2006.

[30] K. Jordan *et al.*, *Fiber-Reinforced-Polymer (FRP) Architectural Products*, 1st ed. Wilson Boulevard, Suite: American Composites Manufacturers Association, 2016.

[31] D. N. Subramanian, "FRP Rebars," *Structural Engineering Forum of India*, 2014. [Online]. Available: https://www.sefindia.org/forum/viewtopic.php?p=66821. [Accessed: 08-Dec-2019].

[32] Z. Carbon, "CFRP Rebar," *CFRP Rebar*, 2015. [Online]. Available: http://www.zacarbon.com/cfrp-rebar. [Accessed: 08-Dec-2019].

[33] F. Elgabbas, E. A. Ahmed, and B. Benmokrane, "Physical and mechanical characteristics of new basalt-FRP bars for reinforcing concrete structures," *Construction and Building Materials*, vol. 95, pp. 623–635, 2015.

[34] P. Mallick, *Fiber Reinforced Composites Materials, Manufaturing and Design*, 3rd ed. Dearborn, Michigan: Taylor and Fracis Group, 2007.

[35] Q. S. Khan, M. N. Sheikh, and M. N. S. Hadi, "Tension and compression testing of fibre reinforced polymer (FRP) bars," in *The 12th Iternational Symposium on FIber Reinforced Polymers for Reinforced Concrete Structures (FRPRCS-12)*, 2015, pp. 1–6.

[36] U. Taketo, M. Hiroshi, K. Futoshi, and M. Sudhir, "Use of Fiber Reinforced Polymer Composites as Reinforcing Material for Concrete-2001.pdf," *Journal of Materials in Civil Engineering*, vol. 14, no. 14, pp. 191–209, 2002.

[37] A. Altalmas, A. El Refai, and F. Abed, "Bond degradation of basalt fiber-reinforced polymer (BFRP) bars exposed to accelerated aging conditions," *Construction and Building Materials*, vol. 81, pp. 162–171, 2015.

[38] ACI Committee 408, *Bond and Development of Straight Reinforcing Bars in Tension*. American Concrete Institute, 2003.

[39] A. El Refai, M.-A. Ammar, and R. Masmoudi, "Bond Performance of Basalt Fiber-Reinforced Polymer Bars to Concrete," *ASCE Journal of Composites for Construction*, vol. 19, no. 3, pp. 1–12, 2015.

[40] W. Wang, D. Jiang, and C. T. Hsu, "Shear Strength of Reinforced Concrete Deep Beams," *Journal of Structural Engineering*, vol. 119, no. 8, pp. 2294–2312, 2015.

[41] B. R. Niranjan and S. S. Patil, "Analysis of R.C Deep Beam by Finite Element Method," *International Journal of Modern Engineering Research*, vol. 2, no. 6, pp. 4664–4667, 2012.

[42] Canadian Standards Association, *Concrete Frame Design Manual*, 1st ed., no.

1. California, United State of America, 2017.

[43] ACI Committee 318, "Building Code Requirements for Structural Concrete (ACI 318-14)," Michigan, 2014.

[44] G. A. Rao, K. Kunal, and R. Eligehausen, "Shear strength of RC deep beams," *The Physical Science Basis*, vol. 2, pp. 1–30, 2007.

[45] C. Elanchezhian, B. V. Ramnath, and J. Hemalatha, "Mechanical Behaviour of Glass and Carbon Fibre Reinforced Composites at Varying Strain Rates and Temperatures," *Procedia Materials Science*, vol. 6, pp. 1405–1418, 2014.

[46] F. Abed and M. Alhamaydeh, "Shear characteristics of GFRP-reinforced concrete deep beams without web reinforcement," *Reinforced Plastics and Composites*, pp. 1–11, 2012.

[47] A. S. Farghaly and B. Benmokrane, "Shear behavior of FRP-reinforced concrete deep beams without web reinforcement," *ASCE Journal of Composites for Construction*, vol. 17, no. 6, pp. 1–10, 2013.

[48] S. Alhamad, Y. Al Banna, A. Al Osman, and J. Mouthassseeb, "Effect of shear span-to-depth ratio on the shear behavior of BFRP-RC deep beams," in *Advances in Sustainable Construction Material and Civil Engineering System*, 2017, vol. 120, pp. 1–7.

[49] Canadian Standards Association, "Design and Construction of Building Components with Fibre-Reinforced Polymers," Toronto, Canada, 2009.

[50] T. Simões, H. Costa, D. Dias-da-Costa, and E. Júlio, "Influence of fibres on the mechanical behaviour of fibre reinforced concrete matrixes," *Construction and Building Materials*, vol. 137, pp. 548–556, 2017.

[51] J. O. Lerch, H. L. Bester, A. S. Van Rooyen, R. Combrinck, W. I. de Villiers, and W. P. Boshoff, "The effect of mixing on the performance of macro synthetic fibre reinforced concrete," *Cement and Concrete Research*, vol. 103, pp. 130–139, 2017.

[52] J. Reis, "Mechanical characterization of fiber reinforced Polymer Concrete," *Materials Research*, vol. 8, no. 3, pp. 357–360, 2005.

[53] J. Branston, S. Das, S. Y. Kenno, and C. Taylor, "Mechanical behaviour of basalt fibre reinforced concrete," *Construction and Building Materials*, vol. 124, pp. 878–886, 2016.

[54] M. S. Issa, I. M. Metwally, and S. M. Elzeiny, "Influence of fibers on flexural behavior and ductility of concrete beams reinforced with GFRP rebars," *Engineering Structures*, vol. 33, no. 5, pp. 1754–1763, 2011.

[55] H. Wang and A. Belarbi, "Ductility characteristics of fiber-reinforced-concrete beams reinforced with FRP rebars," *Construction and Building Materials*, vol. 25, no. 5, pp. 2391–2401, 2011.

[56] M. J. Hasan, M. Afroz, and H. M. I. Mahmud, "An Experimental Investigation on Mechanical Behavior of Macro Synthetic Fiber Reinforced Concrete," *Environmental Engineering*, vol. 11, no. 3, pp. 18–23, 2011.

[57] J. M. Yang, K. H. Min, H. O. Shin, and Y. S. Yoon, “Effect of steel and synthetic fibers on flexural behavior of high-strength concrete beams reinforced with FRP bars,” *Composites Part B: Engineering*, vol. 43, no. 3, pp. 1077–1086, 2012.

[58] D. Chonghai and M. A. Xinwei, “Experimental Research on Mechanical Properties of Basalt Fiber Reinforced Reactive Powder Concrete,” in *International Conference on Advanced Materials and Engineering Materials*, 2013, pp. 2–5.

[59] M. D. Brown and O. Bayrak, “Design of Deep Beams Using Strut-and-Tie Models — Part I : Evaluating U . S . Provisions,” *ACI Structural Journal*, no. 105, pp. 395–404, 2009.

[60] Canadian Standards Association, *Design of Concrete Structures CSA A23.3-04*. Mississauga, Canada, 2004.

[61] J. K. Wight *et al.*, *Building Code Requirements for Structural Concrete and Commentary*. Michigan, United States: American Concrete Institute, 2002.

[62] A. Mello and R. Souza, “Analysis and design of reinforced concrete deep beams by a manual approach of stringer-panel method,” *Latin American Journal of Solids and Structures*, vol. 13, no. 6, pp. 1126–1151, 2016.

[63] M. Moradi and M. R. Esfahani, “Application of the strut-and-tie method for steel fiber reinforced concrete deep beams,” *Construction and Building Materials*, vol. 131, pp. 423–437, 2017.

[64] A. Arabzadeh, A. R. Rahaie, and R. Aghayari, “A Simple strut-and-tie model for prediction of ultimate shear strength of RC deep beams,” *International Journal of Civil Engineering*, vol. 7, no. 3, pp. 141–153, 2009.

[65] ASTM International, “Compressive Strength of Hydraulic Cement Mortars C109/C109M,” American Society for Testing and Materials, Pennsylvania, United States, 2007.

[66] ASTM International, “Standard Test Method for Splitting Tensile Strength of Cylindrical Concrete Specimens C496,” American Society for Testing and Materials, Pennsylvania, United States, 1996.

[67] ASTM International, “Standard Test Method for Flexural Performance of Fiber-Reinforced Concrete C1609-10,” Pennsylvania, United States, 2010.

[68] F. Abed, A. El Refai, and S. Abdalla, “Experimental and finite element investigation of the shear performance of BFRP-RC short beams,” *Structures*, vol. 20, pp. 689–701, 2019.

[69] H. Zhang, L. Wang, L. Bai, M. Addae, and A. Neupane, “Research on the impact response and model of hybrid basalt-macro synthetic polypropylene fiber reinforced concrete,” *Construction and Building Materials*, vol. 204, pp. 303–316, 2019.

[70] A.F. Ashour, “Shear Capacity of Reinforced Concrete Deep Beams,” *Journal of Structural Engineering*, vol. 126, no. 9, pp. 1045–1052, 2000.

Vita

Mohamad Kusay Sabbagh was born in 1993, in Aleppo, Syria. He received his primary and secondary school certificates in Khobar, Saudi Arabia in 2011. After that, he joined University of Sharjah and graduated in 2016 with Bachelor of Science in Civil Engineering.

In September 2016, Mr. Mohamad continued his academic studies in the Civil Engineering master's program at the American University of Sharjah. He enrolled in construction industry by several internships and duties in consulting and contracting companies, while he was completing his master's requirements. His research interests are concentrated in Mechanics of Materials, Concrete Technology, and Sustainability of Structural Elements.